Response to reviewer comments on “Crustal structure of southeast Australia from teleseismic receiver functions” (manuscript se-2020-74) by Bello et al.

We thank the two reviewers for their constructive comments. The revision process has been delayed somewhat due to the lead author being unable to contribute due to health reasons. However, the co-authors feel that the updated version of the manuscript does address the primary comments and concerns of both reviewers, and is a distinct improvement on the original.

Note: Reviewer comments are in Blue text, and author responses are in black text. Line numbers refer to the marked up version of the manuscript.

Reviewer #1

Comment: In the present manuscript, the authors calculated and evaluated Ps receiver functions at a total of 32 seismic stations in southeast Australia, most of them situated along both sides of Bass Strait (Victoria and Tasmania). They applied H-K stacking and receiver function inversion using the neighborhood algorithm, relatively standard techniques that have already been applied to different datasets in E and SE Australia.

The performed processing and analysis was carried out competently, the obtained results appear to be mainly solid, and the manuscript is overall well written. However, I have large reservations about the study’s significance. It basically just provides a few (way fewer than is apparent at first glance, see comments below) new data points that do not really show us anything new, and it also does not attempt to gain new insights by combining the obtained information with other existing evidence in a meaningful and potentially novel way. I thus think that the study should not be published in its current shape, but the authors should be encouraged to submit an extended and improved version of the study that tries to, at least, improve on point 2 of my General comments (see below).
Response: We thank the reviewer for their constructive criticism of the manuscript. We acknowledge that the receiver function results we obtain only represent a portion of the stations for which data are available, but we were very careful to remove poor quality data, and this resulted in fairly substantial culling of the dataset, which is inherently noisy due to the proximity of most stations to Bass Strait and the Southern Ocean. An extensive re-examination of the data has been made in response to this point, including re-processing the receiver functions and a less automated assessment. As a result. we have been able to add an additional four H-κ stacking results for the portable network (stations BA03, BA09, BA19 and BA20) and eight NA inversion results for the portable network (BA02, BA07, BA08, BA09, BA13, BA17, BA19 and BA20) – see the revised Table 2. These new results make a substantial contribution to the revised paper, and has meant that the Abstract, Discussion and Conclusion sections have been substantially modified. We also take the point regarding the exploitation of existing evidence to improve our interpretation, and have put considerable effort towards achieving this in the revised manuscript.

Comment: As mentioned above, my main concern with this paper is its lack of significance. This can be broken down into two problems:

1. Data paucity and lack of novel results
The abstract talks about receiver functions from 32 stations (24 temporary from the BASS deployment, 8 permanent), but H-K results are only supplied for 13 stations(7 temporary, 6 permanent; the text says 14 stations but Table 2 only features 13), inversion results only for 6 (only permanent stations).

What the manuscript does not mention is that Moho depth estimates from receiver functions are already available from literature for 5 of the 6 permanent stations investigated (station CAN in Clitheroe et al., 2000; stations MOO, TOO, TAU, YNG in Ford etal., 2010; all 5 are also used in the AusMoho compilation of Kennett et al., 2011), and vp and vp/vs estimates for 4 of the 6 (Ford et al., 2010). This reduces the amount of new results to H-K stacking results from 7 temporary stations, and H-K stacking plus inversion for one permanent station (CNB) for which I could not find previous results.

This is a rather thin data base, and I think the authors should have mentioned the previous results I just listed, and discussed whether their new values agree or disagree with these previous findings (they are largely consistent, as far as I can see). Failure to do that appears to wrongly imply that all reported values are novel. Comparison is only undertaken with other previously analyzed stations in the region (Figure 9), which adds to this impression. Lastly, it would make sense to compare the obtained crustal thicknesses to the Australia-wide Moho model AusMoho (freely available from the webpage of ANU:http://rses.anu.edu.au/seismology/AuSREM/AusMoho/). This interpolated model offers predictions (interpolated values) for the positions of the newly analysed stations, thus it offers the possibility to check whether these results change or confirm the cur-rent state of knowledge (at first glance, they rather confirm).
Response: We acknowledge that what we wrote could be interpreted as a claim that we obtain receiver functions from all 32 stations, so have added a subsequent sentence that clarifies the actual number of usable receiver functions we extract (see lines 13-15). As noted above, we have re-assessed the temporary station data, and applied different receiver function assessment criteria, which has yielded additional results that we hope will help allay the reviewer's concern regarding data paucity.

In response to the second point, we now make mention of the previous Moho depth estimates for five of the six permanent stations, and show that they are consistent with our results. See lines 398-407.

In response to the last point, we have added a new figure (Figure 11) which compares all of our Moho depth results with AusREM estimates. As the reviewer notes, they are in general quite consistent, but with a few exceptions that we discuss in a new section (7.3) in the manuscript – see lines 560-597.

Comment: 2. Lack of constraints for interpretation
The authors offer a detailed introduction to models of crustal formation and geologic evolution of SE Australia in Sections 1 and 2. I am no expert in these things, but I get the impression that a thorough survey of the literature was performed. The Discussion section then attempts to relate the rather poor data base (see above) to all kinds of geological processes that have been previously proposed. I think the authors are doing an OK job in relating their results to some published works, but the central problem is that the few newly obtained data are mostly interpreted in isolation. It would make a lot of sense to do cross plots with results from other geophysical studies, trying to see more by combining different datasets. This is not done at all, which is even more surprising considering that the first author published two other seismological studies on the same area, even partially using the same stations, last year (Bello et al.,2019a,b; teleseismic tomography and shear-wave splitting). While both of these methods rather illuminate deeper, sub-crustal structure, a combined interpretation would allow a much better discussion and potentially offer novel insights. I wonder why this is not done here, unless the authors want to publish this in yet another paper (which would be slicing it rather thinly). Looking at these previous papers, I also wonder why there was no attempt to use at least some of the huge number of WOMBAT temporary stations that was

harvested for the teleseismic tomography in the present study, to derive some more (novel) data points.

Response: The reviewer makes a fair point with regard to the lack of comparison with the results from other relevant studies. As a consequence, we have made the following changes:

1. As noted above, we now compare our results with the AuSMoho model (Figure 11 and Section 7.3).
2. We also compare our results in Tasmania to the study of Rawlinson et al. (2001) who invert wide-angle traveltimes (both reflection and refraction) for crustal velocity and Moho geometry (see Supplementary Figure S9).
3. We also include a new figure, which provides a joint interpretation of our results from teleseismic tomography, shear wave splitting and receiver function analysis (see Figure 12) and discuss it in detail in a new section (7.4) – see lines 598-623.

With regard to the last point, the WOMBAT stations were all short period stations (1 Hz corner frequency), many were only vertical component, and deployment times were often less than a year. All the Victorian stations and those deployed in northern Tasmania were vertical component, which means that it was not possible to extract receiver functions from them.

Comment: ll.24/25: I found it rather confusing that the authors talk about vp/vs ratio and Poisson ratio separately (here and also in Section 7.2), although these properties are directly related (see Equation 2) and thus one does not offer additional information compared to the other.

Response: We agree with the reviewer's comment, and have revised the manuscript so that it just refers to *Vp/Vs* ratio (see Abstract and Section 7.2).

Comment: ll.54-57: Some parts of a sentence are apparently missing here.

Response: As far as we can tell, the sentence in question appears to be complete. However, we have broken it up into two sentences, which hopefully improves its clarity (see lines 67-71).

Comment: ll.93-100: If VanDieland is just a conceptual microcontental block in one of the models that is routinely used to explain the genesis of the region, why is the term used to reference station locations (e.g. Table 2). Shouldn't geographical regions that are independent of interpretation framework be used for this?

Response: This is a fair point, and we have now removed such references (e.g. Table 2).

Comment: ll.102-154 (Section 3): I personally dislike this type of listing of existing studies, going study by study and explaining the methodology of each. This is unnecessarily bloated and in the end the reader doesn't take away much beyond "people have worked in this area before". It would be better to include the geophysical evidence into the presentation of evolution concepts given in Section 2 (and partly Section 1).

Response: We think it is worthwhile to summarise the results of previous geophysical studies, so have retained this section. However, we do acknowledge the reviewer's point, and therefore have changed it considerably to focus more on the outcomes of these studies. This includes largely removing the first paragraph, which merely lists the range of techniques that have been applied and relevant references. See lines 116-185 of the revised manuscript.

Comment: l.152: part of the sentence is missing (?)

Response: This sentence appears to be complete as far as we can tell.

Comment: ll.174/175: I disagree on this claim

Response: We have deleted this sentence (see lines 221-222).

Comment: l.185: "by using the clarity of the direct arrivals"; was this a purely visual selection or were there fixed criteria? Some more detail would be useful.
Response: We have added “visual clarity” to the sentence in question (see line 240).

Comment: l.208: Although the paper of Zhu and Kanamori (2000) is cited here, the used weighting scheme (0.6/0.3/0.1) is not the same as in that paper (0.7/0.2/0.1).
Response: We have removed the citation (see line 270-271).

Comment: l.213: How robust is the use of standard deviations as uncertainty estimates when there are only 4-6 measurements (as is the case for 5 of the 13 stations, see Table 2)? This should at least be mentioned/discussed.
Response: This is a fair point, and we have added an additional sentence to explain the limitations of this approach (see lines 276-278).

Comment: l.240: "Our strict criteria ...": what were these criteria? It would be worth explaining how this was done, especially since it leads to a reduction from 32 to 6 stations.
Response: We have rephrased this sentence to make it clear that we are using visual criteria for acceptance (see line 305-306).

Comment: l.243: Why have a subchapter 5.3.1 if there is no 5.3.2?
Response: We have removed this heading (see line 308).

Comment: l.294ff: Why is it not even mentioned that there is a huge difference in Moho depth between the two different applied analysis techniques (H-K and inversion) for all (3) stations in the Lachlan Fold Belt that were investigated with both methods (see Table2)? These differences are around 10 km, thus very significant.
Response: We have revisited these Moho picks from the NA inversion, and determined that they were not done correctly. As can be seen in Table 2, they have been changed, with YNG H-κ depth=37 km, NA depth=35km; CAN H- κ depth=39 km, NA depth=40 km; CNB Hκ - depth=38 km, NA depth=39 km. However, it is worth noting that previous RF inversion results have favoured a Moho that is ~10 km deeper beneath this region. We have discussed this in Section 7.1 – see lines 432-440.

Comment: Figures 6 and 9: I find the black-to-white color scale not to be a very good choice here, it is quite hard to see at a glance where e.g. the crust is thick and where thin. A different color scale may be more appropriate.
Response: These figures have been redone using a colour scale that makes it easier to distinguish between thick and thin crust - see Figures 6 and 10.

Comment: Figures 7 and 8: It would be useful to show where the Moho was picked in the shear-wave velocity models. Taking the values from Table 2, I actually disagree with the picks for stations YNG and CAN. In both of these cases, the clearer jump in vs is much shallower than what is listed in Table 2 (around 35 and 40 km instead of 48 and 49km), which would also be much more consistent with H-K results.
Response: The pick locations have now been included in Figures 7-9, noting that we also include two example RF inversions from the temporary array in the new Figure 9. As noted in a previous comment, the original picks for YHG, CAN and CNB were too deep, and have been revised, so the reviewer is correct. However, please also refer to lines 432-440 of the manuscript for an explanation of why the precise Moho depth might be difficult to estimate here.

Reviewer #2

Comment: This carefully researched and well-written contribution places solid constraints on the crustal structure of southeast Australia by the construction and inversion of teleseismic receiver functions underneath a series of high-quality seismic stations. Building on these results for the thickness and sharpness of the crust, the authors put forward a tectonic interpretation, or rather a substantiation of earlier geological theories, involving magmatic underplating, which places the structure of the region into a proper geodynamic context.

I have relatively little to offer in the form of scientific criticism or comments on the seismological methods, which are sound, well-established, and well executed, although I am making a number of suggestions related to the presentation of the materials.

I am judging the paper primarily on its seismological merits, and not on the finer points of the interpretation. My main point related to the interpretation is that the comparison with earlier results by other authors is mostly qualitative, in the form of a color-coded figure, where I would have preferred a more detailed cross-comparison including a statistical analysis of uncertainty. How different can two crustal models made at two nearby stations be before tension develops with the interpretation? How different can two crustal models made at the same station be before we must dig into the details in order to interpret one of them as “better”, or both of them as “equivalent”? The authors leave a bit of material on the table here.

I am attaching a hand-annotated manuscript. I will number and restate my most important comments here. I will not repeat “obvious” but necessary corrections here.

Response: We thank the reviewer for the positive comments, and in the revised manuscript, attempt to improve on the quantitative nature of the comparison with previous results.

Comment: L261 What are those degrees of freedom, how do you determine them? The reference to Gouveia and Scales is too vague.
Response: The degrees of freedom is equal to the number of observations minus the number of inversion parameters, which we now state in the manuscript (see lines 328-329).

Comment: L310 In the same vain. I know it is hard to formally justify, but if you have the right number of degrees of freedom, and you have the right amount of independence in the entries of the summand, the reduced-chi-squared value that you should be aiming for is 1. Are you looking at the distribution of your misfits to establish that they ARE indeed chi-squared distributed? Are you sure that you are using the right amount of degrees of freedom? Are you sure that your lowest chi-squared values are not overly optimistic (as in: that they could be nearly perfect fits to models with too many free parameters).
Response: This is a fair point, and ideally one would be aiming for a value of 1 to fit the data. However, apart from getting the number of degrees of freedom right, the noise estimate is also a factor, and its absolute value is poorly constrained. This may be why the chi-square values are on the low side, but we think it is reasonable to consider our measure of chi-square as a relative indicator of data fit, which we now acknowledge on lines 393-397. It is also worth noting that it is fairly typical of NA RF inversion studies to end up with chi-square misfit values well below 1 (e.g. Wu et al., 2015: Crustal shear wave velocity structure in the northeastern Tibet based on the Neighbourhood algorithm inversion of receiver functions. Geophysical Journal International, **212**, 1920-1931)

Comment: L832 I assume we are talking about the same criterion here, and so the caption should explicitly refer to it.

On the whole, I would like to read more about your misfit criterion, and I would like you to make explicit the now implicit distributional assumptions made about your metric.
Response: Yes, this is the same misfit measure, which is now clarified in the paper (see line 1014).

Comment: L831 I definitely would put the numbers in call-out boxes on the maps also. A color scale is hard to read for some, and any additional clarity that can be gleaned from a multiplicity of representation is to be welcomed.
Response: We now point out the depth values on the plots.

Comment: L835 Let the caption teach us how to read the top and bottom axes in the left-hand panel.
Response: We have changed the caption as requested (see line 1012).

Comment: L850 Again, it is hard to see differences when they are presented on a busy colored map in a smooth gray-scale representation. A table would be nice in the main text. Spell out the differences, attempt to make sense of them relative to their uncertainty and their spatial proximity. Make us confident that your study is not just "another opinion", make us confident that other studies weren't just "another study", in other words:integrate the results of your an other studies and talk us through the similarities and differences. In the text, emphasize the common points and the differences, in particular in light of the interpretation.
Response: We have changed the relevant figures (Figure 6 and 10) to make it easier to read the variations in Moho depth, and changed the discussion to make it more integrated, along the lines suggested by the reviewer. Table 2 also provides a quantitative summary of all our new results.

Comment: L10, L15, L26 "understanding", "this", "explains" -> those are all vague terms. After reading the manuscript it became clear to me that you had more detail in mind, some of which you have room to put into the abstract**.**
Response: We have made some modifications to the Abstract to improve upon clarity.

Comment: L17 "postulated Precambrian continental" -> I propose "putative" if the postulate refers to the fragment being "continental" or "putatively" if it refers to being "Precambrian"**.**
Response: We have implemented this change (see line 21).

Comment: L50, L55 -> Establish a consistent notation and typographical conventions
Response: This has been done.

Comment: L150, L152, L186, L186 -> Fix typos and inconsistencies
Response: This has been corrected.

Comment: L287 "relatively average to high" -> we need a basis for comparison, and a different word than "average" - in my book, values are not "average" unless they are "averages",and you most likely mean that these values are "unremarkable", "usually/frequently observed" (compared to what then?
Response: The paragraph containing this text has been deleted as part of the revisions.

Comment: L325 -> Fix typo/inconsistency
Response: Typo has been corrected.

Comment: L376 There is a lack of referencing in this sentence, which must refer to specific studies for each of the assertions made in it. Also "depicted" is not the greatest choice of word here.

Response: We have replaced “depicted” with “revealed”, and included a reference to the work of Christensen (1996). The reference to Owens and Zandt (1997) in the second point refers to the relationship between partial melt and Poisson’s ratio. See lines 487-489.

Comment: L447 -> Fix typo/inconsistency
Response: Done.

Comment: L777, L788, L791, L809 -> Fix capitalization
Response: Done

Comment: L798 Personally I would leave ETOPO1 out of the caption unless I was willing to put a color scale to it. At this scale and with this projection and without a color scale it’s immaterial what topography model is being used.
Response: We agree, but it is a journal requirement to state the source of any information we use in figures that was obtained from outside the current study.

Comment: L802 I would label the phases with letters on the graph also, right now the colors are not all that distinct on the screen, and they won’t be on a black and white printer or photocopier, either.
Response: This suggestion has been implemented – see Figure 4.

Annotated manuscript: We also implemented the minor hand-annotated suggestions in the manuscript provided by Reviewer 2, which were mainly typos and other straight forward edits.

Crustal structure of southeast Australia from teleseismic receiver functions

Mohammed Bello[1, 2], David G. Cornwell[1], Nicholas Rawlinson[3], Anya M. Reading[4], Othaniel K. Likkason[2]

[1]Department Geology & Geophysics, University of Aberdeen, Aberdeen, UK
[2]Department of Physics, Abubakar Tafawa Balewa University, Bauchi, Nigeria
[3]Department of Earth Sciences, University of Cambridge, UK
[4]School of Natural Sciences (Physics), University of Tasmania, Australia

Correspondence to: Mohammed Bello (mbazare13@yahoo.com)

Abstract. In an effort to improve our understanding of the seismic character of the crust beneath southeast Australia, and~~southeast Australia's enigmatic tectonic evolution~~ how it relates to the tectonic evolution of the region, we analyse teleseismic earthquakes recorded by 24 temporary and 8 permanent broadband stations using the receiver function method. Due to the proximity of the temporary stations to Bass Strait, only 13 of these stations yielded usable receiver functions, whereas seven permanent stations produced receiver functions for subsequent analysis. Crustal thickness, bulk seismic velocity properties and internal crustal structure of the southern Tasmanides – an assemblage of Palaeozoic accretionary orogens that occupy eastern Australia – are constrained by~~ our new~~ H-κ stacking and receiver function inversion,~~ results~~ which point to: (1) a ~~a~~ 39.0~~ ± 0.5~~ km thick crust, a~~ relatively~~ n intermediate-high *Vp/Vs* ratio~~high Poisson's ratio~~ (~1.70-1.76)~~0.262 ± 0.014),~~ relative to ak135, and a broad (>10 km) crust-mantle transition beneath the Lachlan Fold Belt. These results are interpreted~~is is interpreted~~ to represent magmatic underplating of mafic materials at the base of the crust; (2) a complex crustal structure beneath VanDieland, a putative~~ostulated~~ Precambrian continental fragment embedded in the southernmost Tasmanides, ~~where the crust thickens (37.5 ± 1.2 km) towards the northern tip of the microcontinent as it enters south central Victoria but thins south into Bass Strait (30.5 ± 2.1 km), before once again becoming thicker beneath western Tasmania (33.5 ± 1.9 km).~~which features strong variability in crustal thickness (23-37 km) and *Vp/Vs* ratio (1.65-193), the latter of which likely represents compositional variability and the presence of melt. ~~The thinner crust beneath Bass Strait can be attributed to lithospheric stretching that resulted from the break-up of Antarctica and Australia and the opening of the Tasman Sea;~~ The complex origins of Vandieland, which comprises multiple continental ribbons, coupled with recent failed rifting and intraplate volcanism, likely contributes to these observations; and (3) stations located in the East Tasmania Terrane and ~~e~~Eastern Bass Strait (ETT+EB) collectively indicate crust of uniform thickness (31-32~~~33~~ km), ~~and a slightly broad Moho transition that reflect a possible underplating event associated with a Palaeozoic subduction system~~which clearly distinguish it from VanDieland to the west. ~~The relative uniformity of *Vp/Vs* and Poisson's ratio in VanDieland – suggesting uniformity in composition – could be used in support of the VanDieland microcontinental model that explains the tectonic evolution of southeast Australia.~~ Moho depths are also compared with the continent-wide AusMoho model in southeast Australia, and are shown to be largely consistent, except in regions where AusMoho has few constraints (e.g. Flinders Island). A joint interpretation of the new results with ambient noise, teleseismic tomography and teleseismic shear wave splitting anisotropy, helps provide new insight into the way that the crust has been shaped by recent events, including failed rifting

during the break-up of Australia and Antarctica and recent intraplate volcanism.

Keywords: receiver functions, crustal structure, VanDieland, Bass Strait, SE Australia

1 Introduction

The Phanerozoic Tasmanides (Collins and Vernon, 1994; Coney, 1995; Coney et al., 1990) comprise the eastern one-third of the Australian continent and through a process of subduction accretion were juxtaposed against the eastern flank of the Precambrian shield region of Australia beginning in the Late Neoproterozoic and Early Palaeozoic (Foster and Gray, 2000; Glen, 2005; Glen et al., 2009; Moresi et al., 2014) (Figure. 1). Persistent sources of debate that impede a more complete understanding of the geology of the Tasmanides include: (1) the geological link between Tasmania – an island state in southeast Australia – and— mainland Australia, which are separated by the waters of Bass Strait; and (2) the presence and locations of continental fragments from Rodinian remnants that are entrained within the accretionary orogens. Furthermore, the lateral boundaries between individual tectonic blocks and their crustal structure are often not well defined. To date, few constraints on crustal thickness and seismic velocity structure have been available for regions such as Bass Strait. Constraints on the Moho transition, crustal thickness and velocity structure beneath Bass Strait derived from receiver functions (RFs) can therefore provide fresh insight into the nature and evolution of the Tasmanides.

Previous estimates of crustal thickness and structure beneath southeastern Australia have been obtained from deep seismic reflection transects, wide-angle seismic data, topography and gravity anomalies (e.g. Collins, 1991; Collins et al., 2003; Drummond et al., 2006 and Kennett et al., 2011). Earlier RF studies in southeast Australia (Shibutani et al., 1996; Clitheroe et al., 2000; Tkalčić et al., 2011; Fontaine et al., 2013a,b) suggested the presence of complex lateral velocity variations in the mid-lower crust that probably reflect the interaction of igneous underplating, associated thinning of the lithosphere, recent hotspot volcanism and uplift. Furthermore, the intermediate to high crustal *Vp/Vs* ratio of 1.70–1.78 in this region (Fontaine et al., 2013a), relative to ak135 continental crust where *Vp/Vs* is ∼1.68, may indicate a mafic composition that includes mafic granulite rocks, granite-gneiss and biotite gneiss. Body- and surface-wave tomography (Fishwick and Rawlinson, 2012; Rawlinson et al., 2015) revealed *P* and *S* wave velocity anomalies in the uppermost mantle beneath Bass Strait and the Lachlan Fold Belt. Ambient noise surface wave tomography (Bodin et al., 2012b; Young et al., 2012; Pilia et al., 2015b, 2016; Crowder et al., 2019) of the southern Tasmanides revealeds significant crustal complexity, but is unable to constrain crustal thickness or the nature of the Moho transition.

The goal of this paper is to provide fresh insight into the crust and Moho structure beneath the southern Tasmanides using *P*-wave RFs and explain the origin of the lateral heterogeneities that are observed. This will allow us to and explore the geological relationship between the different tectonic units that constitute the southern Tasmanides, and yielddevelop an improved understanding of the region's tectonic history.thereby facilitating a better grasp of the region's tectonic history.

2 Geological setting

The Palaeozoic-Mesozoic Tasmanides of eastern Australia form part of one of the most extensive accretionary orogens in existence and evolved from interaction between the East Gondwana margin and the Proto-Pacific

Ocean. The tectonic evolution of the Tasmanides is complex and large-scale reconstructions have proven difficult. This is evident from the variety of models that have been suggested to explain how the region formed (Foster and Gray, 2000; Spaggiari et al., 2003; Teasdale et al., 2003; Spaggiari et al., 2004; Boger and Miller, 2004; Glen, 2005; Cawood, 2005; Glen et al., 2009; Cayley, 2011a,b; Gibson et al., 2011~~1,~~; Moresi et al., 2014; Pilia et al., 2015a,b). Particular challenges arise from multiple subduction events, multiple phases of metamorphism, entrainment of exotic continental blocks, the formation of large oroclines, recent intraplate volcanism and subsequent events, including the separation of Antarctica and Australia and the formation of the Tasman Sea. These challenges are compounded by the presence of widespread sedimentary sequences that hinder direct access to basement rocks (Fig. 1).

The Tasmanides consist of four orogenic belts, namely the Delamerian, Lachlan, Thomson and New England Orogens. The Delamerian Orogen - located in the south - is the oldest part of the Tasmanides and has a southward extension across Bass Strait from Victoria into western Tasmania, where it is commonly referred to as the Tyennan Orogen (Berry et al., 2008). Between about 514 and 490 Ma, the Precambrian and Early Cambrian rocks that constitute the Delamerian Orogen were subjected to a contractional orogenic event along the margin of East Gondwana (Foden et al., 2006). Subsequently, the Lachlan Orogen formed in the east, which contains rocks that vary in age from Ordovician to Carboniferous (Glen, 2005). Gray and Foster (2004) argued for a tectonic model ~~for~~of the Lachlan Orogen that involved interaction of a volcanic arc, oceanic microplates, several turbidite thrust systems and three distinct subduction zones. Each subduction zone is linked to the formation of a distinct tectonic terrain: the Stawell-Bendigo zone, Tabbarebbera zone and Narooma accretionary complex. The limited rock exposure in the Tasmanides as a whole has made direct observation of the Lachlan Orogen difficult; this is attributed to a large swath of Mesozoic-Cenozoic sedimentary cover and more recent Quaternary volcanics, which obscure a large portion of the underlying Palaeozoic terrane. However, the Lachlan Orogen contain belts of Cambrian rocks in Victoria and New South Wales that are similar in age to the Delamerian Orogen~~,~~ (Gray and Foster, 2004).

The presence of Precambrian outcrops in Tasmania and the relative lack of similar age rocks in adjacent mainland Australia has led to different models which attempted to explain the existence of Proterozoic Tasmania. For instance, Li et al. (1997) suggested that western Tasmania may be the remnant of a continental fragment set adrift by Rodianian break-up, whereas Calvert and Walter (2000) proposed that King Island, along with western Tasmania, rifted away from the Australian craton around ~600 Ma (Fig. 1). Other researchers have developed scenarios in which the island of Tasmania was present as a separate microcontinental block that was positioned outboard of the eastern margin of Gondwana before re-attaching at the commencement of the Palaeozoic (Berry et al., 2008).

A popular model that attempts to reconcile the geology observed in Tasmania and adjacent mainland Australia is that of Cayley (2011a). This model proposes that central Victoria and western Tasmania formed a microcontinental block called “VanDieland” that fused with East Gondwana at the end of the Cambrian, possibly terminating the Delamerian Orogeny. VanDieland became entangled in the subduction-accretion system ~~that~~which built the Palaeozoic orogens~~–~~ that now comprise eastern Australia (Fig. 1). Delineating Precambrian continental fragments within southeast Australia has proven difficult, partly due to more recent

sedimentary cover that obscures large tracts of the Tasmanides. However, if present, they likely have distinctive structural and seismic velocity characteristics (Glen, 2013).

3 Previous geophysical studies

A variety of geophysical methods have so far been deployed to study the ~~Imaging techniques previously employed to study crustal structure~~ crustal structure of ~~beneath~~ the Tasmanides. ~~include: RF analysis (e.g. Shibutani et al., 1996; Clitheroe et al., 2000; Chevrot and van der Hilst, 2000; Kennett et al., 2011; Fontaine et al., 2013a,b), ambient noise tomography (e.g. Saygin and Kennett, 2010; Bodin et al., 2012b; Young et al., 2013a,b; Pilia et al., 2015a,b; Crowder et al., 2019), studies based on potential field imaging and numerical modelling (e.g. Gunn et al., 1997; Morse et al., 2009; Moresi et al., 2014; Moore et al., 2015, 2016), teleseismic tomography (Rawlinson and Urvoy, 2006; Rawlinson and Kennett, 2008; Rawlinson et al., 2015, 2016; Bello et al., 2019b) and seismic reflection and refraction profiling (e.g. Finlayson et al., 1980; Collins, 1991; Direen et al., 2001; Glen et al., 2002; Finlayson et al., 2002; Drummond et al., 2006; Cayley et al., 2011; Glen, 2013).~~ Shibutani et al. (1996) applied a non-linear inversion method to RF waveforms to constrain the shear wave velocity beneath broadband seismic stations in eastern Australia. They found that the Moho is relatively shallow (30-36 km depth) and sharp within the cratonic region, and deeper (38-44 km) and transitional along the axis of the Tasmanides. They suggested that crustal thickening of the fold belt by underplating or intrusion of mantle materials may have contributed to this observation. ~~The work of~~ Clitheroe et al. (2000) built on this earlier work by inverting ~~used~~ RFs to map broad-scale crustal thickness and Moho character across the Australian continent. They found that in general, there was good agreement between xenolith-derived estimates of Moho depth and those determined by RF inversion, except beneath the Lachlan Fold Belt, where a broad Moho transition may be present. Overall, however, the RF results were consistent with those determined by ~~These findings confirmed the previous work of~~ Drummond and Collins (1986) and Collins (1991), who used seismic reflection and refraction ~~-~~ transects to determine that the Lachlan Fold Belt includes ~~has~~ the thickest crust (~50 km) in eastern Australia. ~~Shibutani et al. (1996) applied a genetic algorithm inversion, a non-linear global optimisation technique, to determine the lithospheric velocity structure of southeast Australia from teleseismic RFs. They found that the Moho is shallow (30-36 km) and sharp within the craton and deep (38-44 km) and transitional beneath the Tasmanides. They suggested that underplating or intrusion of mantle material may have thickened the crust and produced a less distinct contrast across the Moho.~~ A more recent study by Fontaine et al. (2013a) employed *H-κ* stacking and non-linear RF inversion to investigate crustal thickness, shear wave velocity structure, as well as dipping and anisotropy of the crustal layers. Their results also indicated a thick crust (~48 km) and an intermediate (2-9 km) crust-mantle transition beneath the Lachlan Fold Belt, ~~zone~~ which could be attributed to underplating beneath the crust and/or high concentrations of mafic rocks in the mid-lower crust. Their results also showed a dipping Moho together with crustal anisotropy in the vicinity of three seismic stations (YNG, CNB and CAN). ~~In our new work, we have a much increased data coverage of the study area (southern Tasmanides); this allows us to resolve new features, and further investigate the presence of structures that have been suggested by previous studies.~~

Over the last decade, ambient noise tomography has become a popular tool for studying the structure of the Australian crust. Saygin and Kennett (2010) produced the first group velocity maps of the Australian continent

from Rayleigh wave group velocity dispersion in the period range 5.0–12.5 seconds. Limited spatial resolution (~ 2° x 2°) in our study region means that this model is only able to represent the structure beneath Bass Strait as a broad, low velocity anomaly. However, the group velocities exhibit a good correlation with known basins and cratons. Subsequent studies using denser arrays covering southeast mainland Australia (Arroucau et al., 2010), southeastern Australia (Young et al. 2013), and northern Tasmania (Young et al., 2011) show good correlations between group/phase velocity maps and sedimentary and basement terrane boundaries. In order to account for uneven data distribution, Bodin et al. (2012b) used a Bayesian transdimensional inversion scheme to generate group velocity maps that span the Australian continent from multi-scale ambient noise datasets. However, in our study area their model is of low resolution due to the limited station coverage and hence few details on crustal structure can be inferred. Bodin et al. (2012a) subsequently applied Bayesian statistics to reconstruct the Moho geometry~~depth~~ of Australia using a variety of seismic datasets, which gave an approximate Moho depth of ~30 km beneath Bass Strait. Pilia et al. (2015a,b) and Crowder et al. (2019) derived 3-D shear wave velocity models of the Bass strait region using ambient noise data from the same array of temporary stations that we exploit in this study. They were able to constrain the lateral and depth extent of the primary sedimentary basins in the region, and provide insight into the seismic character of the Precambrian micro-continental block that appears to underpin southern Victoria, north western Tasmania and Bass Strait.

Teleseismic tomography has also been used to image the lithosphere beneath southeast Australia, thanks in part to the prolific deployment of short-period seismometers as part of the WOMBAT transportable array project (Rawlinson and Kennett, 2008, Rawlinson et al., 2015, 2016). While the main focus has been on the upper mantle, in Tasmania, where station spacing was denser, some constraints on crustal velocity structure were possible. Rawlinson et al. (2006) found that the crust beneath the ETT was significantly faster than the crust beneath central Tasmania, which may represent a contrast between crust with oceanic provenance in the east and Precambrian continental provenance in the west. Bello et al. (2019b) built on this work by including teleseismic arrival time data from the same temporary deployment as the the current study to generate a detailed upper mantle model of southeast Australia, which revealed that Bass Strait was underlain by lower velocities, consistent with thinned lithosphere as a result of failed rifting during the break-up of Australia and Antarctica.

Active source seismic profiling has also been widely used in southeast Australia to characterize crustal velocity structure (e.g. Finlayson et al., 1980; Collins, 1991; Finlayson et al., 2002; Drummond et al., 2006; Glen, 2013). This has largely focused on the transition from continental to oceanic crust at passive margins, but has also been used to image major transition zones or faults between orogens (Glen, 2013) or within orogens (Cayley et al., 2011a,b), the latter of which lead to the VanDieland microcontinental model. Rawlinson and Urvoy (2006) jointly inverted teleseismic arrival times and active source wide-angle traveltimes in northern Tasmania to constrain crustal velocity, Moho geometry and upper mantle velocity structure and found that both northeastern and northwestern Tasmania is characterised by thinner (<28 km) and higher velocity crust compared to central Tasmania.

Potential field data have also been exploited to study the formation and structure of the Tasmanides. Gunn et al. (1997) integrated potential field data (magnetic and gravity), seismic reflection data, outcrop geology and well information to study the crustal structure of the Australian continent. Their study found that the occurrence of

tensional stress, oriented NE-SW along basement structures in the Bass Basin, is able to explain the formation of the three major sedimentary basins that overlie dense mafic material, which in turn was formed by mantle decompression processes associated with crustal stretching. From the interpretation of new aeromagnetic data, Morse et al. (2009) delineated the architecture of the Bass Strait basins and their supporting basement structure. Subsequent studies by Moore et al. (2015, 2016) used gravity, magnetic, seismic reflection and outcrop data to support the hypothesis of a VanDieland microcontinent. Their study showed that VanDieland comprises seven distinct microcontinental ribbon terranes that appear to have amalgamated by the Late Cambrian, with major faults and suture zones bonding these ribbon terranes together.

While the last few decades haves seen important advances and insights made into our understanding of the southern Tasmanides, there still remains limited data on the deep crustal structure beneath Bass Strait, which is our region of interest. It is therefore timely that we can exploit, using the RF technique, teleseismic data recorded by a collection of temporary and permanent seismic stations in the region to study the structure of the crust, Moho and uppermost mantle beneath mainland Australia, Bass Strait and Tasmania.

4 Data

A collaboration involving five organisations (University of Tasmania, Australian National University, Mineral Resources Tasmania, the Geological Survey of Victoria and FROGTECH) deployed the temporary Bass seismic array from May 2011 to April 2013. It consisted of 24 broadband, three-component seismic stations that spanned northern Tasmania, and a selection of islands in Bass Strait and southern Victoria. The instruments used were 23 Güralp 40T and one Güralp 3ESP sensors coupled to Earth Data PR6-24 data loggers. The permanent stations consist of eight broadband sensors managed by IRIS, GEOSCOPE and the Australian National Seismic Network (ANSN). The distribution of all 32 seismic stations that are used in this study is plotted in Figure 2. Earthquakes with magnitudes m_b > 5.5 at epicentral distances between 30° and 90° comprise the seismic sources used in this analysis (Fig. 3). This resulted in an acceptable azimuthal coverage of earthquakes between the northwest and east of the array, where active convergence of the Australian and Eurasian plate coupled with westward motion of the Pacific plate has produced extensive subduction zones. To the south and southwest of the array, the absence of subduction zones in the required epicentral distance range means that there are significantly fewer events available for analysis from these regions.

5 Methods

5.1 Receiver functions

The RF technique (Langston, 1979) uses earthquakes at teleseismic distances to enable estimation of Moho depth and shear wave velocity structure in the neighbourhood vicinity of a seismic recorder. If this technique can be applied to a network of stationss with good spatial coverage, it represents an effective way of mapping lateral variations in Moho depth and crustal structure. The coverage and quality of broadband data available for this study provides a sound basis on which to examine the crustal structure of the southern Tasmanides.

A recorded teleseismic wavefield at a broadband station can be described by the convolutional model in which operators that represent the source radiation pattern, path effects, crustal structure below the station and

instrument response are combined to describe the recorded waveform. By using deconvolution to remove the effects of the source, path and response of the instrument (e.g. Langston, 1979), information on local crustal structure beneath the station can be extracted from *P*-*S* wave conversions at discontinuities in seismic velocity (Owens et al., 1987; Ammon, 1991).

P-wave RFs were determined from teleseismic *P*-waveforms using FuncLab software (Eagar and Fouch, 2012; Porritt and Miller, 2018), following preprocessing using the seismic analysis code (SAC) (Goldstein et al., 2003). RFs were computed by applying~~using~~ an iterative time-domain deconvolution scheme developed by Ligorria and Ammon (1999) with a 2.5 s Gaussian filter width. This is achieved by deconvolution of the vertical component waveform from the radial and transverse waveforms with a central frequency of ~1 Hz. This frequency was selected on account of significant source energy detected in the ~1 Hz range of teleseismic *P* arrivals, which are sensitive to crustal-scale anomalies. It also provides a favourable lateral sensitivity with respect to Fresnel zone width (~15 km at Moho depth) when the conversions from *P* to *S* are mapped as velocity and crustal thickness variations.

~~T~~The complete set of 1765 events (Fig. 3) and 32 stations produced 21,671 preliminary RFs. These RFs were manually ~~picked~~ inspected using the FuncLab trace editor~~,~~ and a subset of 9,674 RFs were selected for further analysis ~~by~~ using the visual clarity of the direct arrivals as an ~~acceptance criteria~~acceptance criterion~~, only a total of 9,674 RFs were retained for further analysis~~. ~~The RFs were computed using an iterative time-domain deconvolution scheme developed by Ligorria and Ammon, (1999) with a 2.5 s Gaussian filter width. This is performed by deconvolution of the vertical component waveform from the radial and transverse waveforms with a central frequency of 1 Hz. This frequency was selected on account of significant source energy detected in the 1 Hz range of teleseismic *P* arrivals, which are sensitive to crustal-scale anomalies. It also provides a favourable lateral sensitivity with respect to Fresnel zone width (~15 km at Moho depth) when the conversions from *P* to *S* are mapped as velocity and crustal thickness variations.~~

Due ~~The~~to high noise levels ~~of noise~~and fewer events associated with the temporary BASS array dataset, a~~and the~~ modest number of good quality RFs ~~we were~~resulted from the ~~able to extract~~above selection method, so different selection criteria were applied that assessed the *P*-arrival, Moho conversion and later amplitudes in conjunction with overall noise levels exhibited by the transverse component RFs. This enabled the temporary BASS stations to yield between 2 and 30 good quality receiver functions, and increased the number of stations where H-κ stacking and NA inversion could be applied from 13 to 20.

5.2 *H*-*κ* stacking

Having obtained reliable *P*-wave RFs, the *H*-*κ* stacking technique is used to estimate crustal thickness~~, Poisson's ratio~~ and bulk *Vp/Vs* for individual stations. We apply the method of Zhu and Kanamori (2000) to stations where the direct *Ps* (Moho *P*-to-*S* conversion) phase and its multiples are observed. This technique makes use of a grid search to determine the crustal thickness (*H*) and *Vp/Vs* (*κ*) values that correspond to the peak amplitude of the stacked phases. A clear maximum requires a contribution from both the primary phase (*Ps*) and the associated multiples (*PpPs* and *PpSs*~~+~~*PsPs*). In the absence of multiples, the maximum becomes smeared out due to the inherent trade-off between crustal thickness (*H*) and average crustal velocity properties (*κ*)~~–~~ (Ammon

et al., 1990; Zhu and Kanamori, 2000). The *H-κ* stacking algorithm reduces the aforementioned ambiguity by summing RF amplitudes for *Ps* and its multiples - *PpPs* and *PpSs+PsPs* - at arrival times corresponding to a range of *H* and *Vp/Vs* values. In the *H-κ* domain the equation for stacking amplitude is

$$s(H,\kappa)=\sum_{j=1}^{N} w_1 r_j(t_1)+w_2 r_j(t_2)+w_3 r_j(t_3) \quad (1)$$

where $r_j(t_i)$; i=1,2,3 are the RF amplitude values at the expected arrival times t_1, t_2, t_3 of the *Ps*, *PpPs*, *PpSs+PsPs* phases respectively for the j^{th} RF, w_1, w_2, w_3 are weights based on the signal to noise ratio, ($w_1+w_2+w_3$=1), and *N* is the total number of radial RFs for the station. ***s****(H,κ)* achieves its maximum value when all three phases stack constructively, thereby producing estimates for *H* and *Vp/Vs* beneath the station (see Figure 5 and Supplementary Figures ~~XXX~~S1-S~~3~~4). In this study, the weighting factors used are w_1=0.6, w_2=0.3, w_3=0.1. ~~and~~ The *H-κ* approach requires an estimate of the mean crustal *P*-wave velocity, which is used as an initial value. Based on the results of a previous seismic refraction study (Drummond and Collins, 1986), we use an average crustal velocity of *Vp* = 6.65 km/s to obtain our estimates of *H* and *κ* in the study area, noting that *H-κ* stacking results are much more dependent on *Vp/Vs* than *Vp* (Zhu and Kanamori, 2000). To estimate the uncertainties in the *H-κ* stacking results, we compute the standard deviation of the *H* and *κ* values at each station. When only a small number of RFs are available at a station (e.g. 4 in the case of MILA) the estimates are unlikely to be particularly robust, and in such instances are perhaps best viewed as a lower bounds on uncertainty.

~~*H-κ* stacking can also be used to determine Poisson's ratio, which is a useful parameter for inferring the physical and compositional properties of the crust (Christensen, 1996) and providing insight into fractures, fluids, and partial melt (e.g. Mavko, 1980). The Poisson's ratio *σ* can be determined from *κ* using the equation~~

~~where *κ = Vp/Vs*.~~ While simple to implement, the Zhu and Kanamori (2000) method can suffer from large uncertainties due to its assumption of a simple flat-laying layer over a half-space with constant crustal and upper mantle properties. Consequently, there are only two search parameters (*H* and *κ*) plus *a priori* information (*Vp*, weightings) and it does not account for variation with backazimuth. These problems can cause non-unique and inaccurate estimates, which can lead to potentially misleading interpretations; for ~~instance~~instance, a low velocity upper crustal layer can appear as a very shallow Moho in an *H-κ* stacking search space diagram. Also, a dipping Moho and/or anisotropic layers within the crust can contribute to uncertainty.

5.3 Nonlinear waveform inversion

In an effort to refine the crustal model, we invert a stack of the radial RFs by adopting the workflow described by Shibutani et al. (1996). We divide the waveform data (RFs) into four 90° quadrants based on the backazimuth of their incoming energy. The 1st quadrant backazimuth range is from 0° and 90°, and an equivalent range in a clockwise direction defines the consecutive quadrants. The 2nd and 3rd quadrants (south-eastern and south-western backazimuths) have very small numbers of RFs. Data from the 1st and 4th quadrants are of better quality, with the 1st quadrant showing more coherency than the 4th quadrant, which is likely due to

the orientation of surrounding tectonic plate boundaries and hence the pattern of *P*-wave energy radiated towards Australia. Kennett and Furumura (2008) showed that seismic waves arriving in Australia from the northern azimuths undergo multiple scattering but low intrinsic attenuation due to heterogeneity in the lower crust and mantle; this tends to produce prolonged high-frequency coda. An important assumption in our inversion is that we neglect anisotropy and possible Moho dip, which we assume have a second order influence on the waveforms we use to constrain 1-D models of the crust and upper mantle.

Visual examination of coherency in *P* to *S* conversions allows us to select a subset of RF waveforms for subsequent stacking. This resulted in groups of mutually coherent waveforms after which a moveout correction is then applied to remove the kinematic effect of different earthquake distances prior to stacking using a cross-correlation matrix approach described in Chen et al. (2010) and Tkalčić et al. (2011). Our ~~strict criteria give reliable~~visual acceptance criteria yields RFs at only 16~~-~~4 out of the 32 stations used for this study. An example of some stacked RFs is given in Fig~~-~~ure 4.

~~5.3.1 Neighborhood algorithm~~

We invert RFs for 1-D seismic velocity structure beneath selected seismic stations using the Neighbourhood Algorithm or NA (Sambridge, 1999a,b) in order to better understand the internal structure of the crust and the nature of the transition to the upper mantle. NA makes use of Voronoi cells to help construct a searchable parameter space, with the aim of preferentially sampling regions of low data misfit. In the inversion process, a Thomson-Haskell matrix method (Thomson, 1950 and Haskell, 1953) was used to calculate a synthetic radial RF for a given 1-D (layered) structure. During the inversion, as in Shibutani et al. (1996) and Clitheroe et al. (2000), each model is described by six layers: a layer of sediment, a basement layer, an upper crust, middle crust and lower crust, and an underlying mantle layer, all of which feature velocity gradients and potentially, velocity jumps across boundaries. The inversion involves constraining 24 parameters: *Vs* values at the top and bottom of each layer, layer thickness and the *Vp/Vs* ratio in each layer (Table 1). The inclusion of *Vp/Vs* ratio as an unknown primarily aims to accommodate the effects of a sediment layer with limited prior constraints (Bannister et al., 2003). There are two important controlling parameters required by NA: (1) the number of models produced per iteration (n_s)~~(~~; and (2) the number of neighbourhoods re-sampled per iteration (n_r). After a number of trials we chose the maximum number of iterations to be 5500, with n_s=13 ~~-~~and n_r=13~~-~~ for all iterations. We employ a chi-squared χ^2~~-~~ metric (see Sambridge 1999a for more details) to compute the misfit function, which is a measure of the inconsistency between the true ϕ_i^{obs} ~~-~~, and predicted, $\phi_i^{pre}(m)$ ~~)~~ waveforms for a given model m :

$$\chi_v^2(m) = \frac{1}{v}\sum_{i=1}^{N_d}\left(\frac{\phi_i^{obs} - \phi_i^{pre}(m)}{\sigma_i}\right) \quad (2)$$

where σ_i represents the noise standard deviation determined from ϕ_i^{obs} , following the method described in

Gouveia and Scales (1998), and ν represents the number of degrees of freedom (the difference between the number of observations and the number of parameters being inverted for). Using the above stated parameters, the inversion targets the 1-D structure that produces the best fit between the predicted and observed RF. Figures 7-9 and 8 and Supplementary Figures S5-S8 present example results of inversions via density plots of the best 1000 data-fitting *S*-wave velocity models produced by the NA. The optimum data fitting model is plotted in red.

6 Results

6.1 *H-κ* stacking results for Moho depth and *Vp/Vs (including Poisson's ratio)*

Maps which plotdepictingof crustal thicknesses and average *Vp/Vs* from H-κ stacking in southeast Australia from 16 stations are plotted from the results obtained at 14 stations (shown in Figure 6 and 9). At the remaining stations, we could not detect any clear multiples or Moho conversions in the RFs from any direction. A previous study by Chevrot and van der Hilst (2000) has noted that this region is devoid of clear multiples. The crustal thickness for all analysed stations in the study area varies from 2330.20 ± 52.01 km (BA02~~11~~) beneath King island in Bass StraitNW Tasmania to 39.1 ± 0.5 km (CAN) beneath the Lachlan Fold Belt, and the variation strongly correlates with topography. The associated *Vp/Vs* values range from 1.65 ± 0.07 (BA11) beneath King island to 1.76 ± 0.04 (YNG) beneath the Lachlan Fold Belt. Crust of the order of 30–34 km thickness occurs beneath much of VanDielandbeneath VanDieland (Fig. 6a) is thin in the north (~37.5 km) and south (~33 km), but appears to be considerably thinner beneath the Victorian and Tasmanian margin of Bass Strait (~25 km). The mountainous region of the Lachlan Fold Belt has the deepest Moho at 39.1 ± 0.5 km (CAN) and a corresponding ***Vp/Vs*** value of 1.73 ± 0.02. Crust that is consistently between ~31 and ~3333 km thick lies beneath the East Tasmania Terrane and Eastern Bass Strait (ETT+EB). *Vp/Vs* ratio varies between ~1.65 beneath station BA11, which also exhibits the thinnest crust, and ~1.93 beneath stations BA19 and BA20 in southern Victoria. There is no obvious correlation between the number of RFs used in the H-κ stacking and the size of the uncertainty in either Moho depth or *Vp/Vs*, but as mentioned previously, the uncertainty estimates for stations with a low number of RFs are likely to be less robust. Table 2 showsis a summary of *H-κ* stacking resultsparameters for the analysed stations that have been analysed.

At ~40 km, the crustal thickness beneath the Lachlan Fold Belt is significant, but decreases southward towards VanDieland (~32.5 km) and southeastward towards the East Tasmania Terrane and Eastern Bass Strait (ETT+EB) (~33 km). Overall, the Moho becomes shallower from the southern tip of VanDieland (TAU) towards and into Bass Strait to the north, before becoming deeper once more under the mainland part of the VanDieland microcontinental block (Fig. 6a). The crustal thickness is more or less uniform beneath the Lachlan Fold Belt, East Tasmania Terrane and eastern Bass Strait.

The majority of our study region has a low-to-intermediate Poisson's ratio. Poisson's ratio is highest (0.262 ± 0.014) in the Lachlan Fold Belt (see Table 2). In VanDieland, the Poisson's ratios generally decrease northward into Bass Strait from 0.240 ± 0.019 (MOO) to 0.210 ± 0.013 (BA11) and then increase into mainland Australia to 0.226 ± 0.017 (TOO). The relatively average to high values in the Lachlan Fold Belt (0.235 ± 0.017 – 0.262 ± 0.014) are in agreement with the presence of a mafic lower crust, as suggested by a number of other studies

~~(Drummond and Collins, 1986; Shibutani et al., 1996; Clitheroe et al., 2000; Finlayson et al., 2002). The ratios in the ETT+EB (0.220 ± 0.008 (BA08) – 0.242 ± 0.005 (BA17)) agree with constraints from seismic reflection and refraction studies and may indicate a felsic to intermediate (average) crustal composition (Finlayson et al., 2002; Collins et al., 2003).~~

6.2 Nonlinear inversion results

Results of the NA inversion were successfully obtained for a selection of permanent and temporary stations, as shown in Table 2 and Figure 10. If the Moho is defined by a gentle velocity gradient, the base of the velocity gradient is used as a proxy for the Moho depth, as done in previous RF (e.g. Clitheroe et al., 2000; Fontaine et al., 2013a) and seismic refraction– (Collins, 1991; Collins et al., 2003) studies. We also adopt an upper mantle velocity of Vp = 7.6 km/s (i.e. Vs = 4.3-4.4 km/s for Vp/Vs ratios of 1.73-1.77 at the base of the Moho gradient) following Clitheroe et al. (2000) who used this value for RF studies, and Collins et al. (2003) who used $Vp > 7.8$ km/s for their summary of both seismic refraction and RF results; these Vp values are consistent with global Earth models (e.g. Kennett et al., 1995). Therefore, we also require the S-wave velocity to be >~4.4 km/s beneath the Moho. We present the S-wave velocity profiles from the NA inversion for stations CAN, MOO, TOO ~~and~~, YNG, BA13 and BA17 in Figures ~~7 and 8~~9, together with observed and predicted RFs. The S-wave velocity inversion results of the remaining ~~two~~ stations are included as supplementary material (see Supplementary Figures S~~4~~5-S8). In assigning the Moho depth, we consider three criteria to examine the quality of the inversion result: (1) misfit value χ^2 ; (2) the quality of the RF stack (which is based on our ability to pick the direct and multiple phases); and (3) the visual fit between the synthetic and observed RF. Models that fail to fit significant arrivals in the observed RF are rejected. Based on these criteria, the inversion results are classified as:

- Very good: very low χ^2 (typically < 0.4), very good visual fit to direct and multiple phases.

- Good: low χ^2 (typically 0.4-0.8), direct phases clearly visible, multiple phases less clear, and a good visual fit to all major identifiable phases.

- Poor: medium to high χ^2 (in the range 0.8-1.2), direct phases visible, multiple phases unclear, and moderate visual fit to some identifiable phases. Looking at the character of the crust-mantle transition, this study classifies the transition zone as sharp ≤ 2 km, intermediate 2-10 km or broad ≥ 10 km as initially proposed by Shibutani et al. (1996) and modified by Clitheroe et al. (2000).

In general, the optimum χ^2 value is normally considered to be 1, since below this value, the tendency is to fit noise rather than signal. However, this is for the ideal case when the number of degrees of freedom and the absolute values of the data uncertainty are well known (e.g. in the case of a synthetic test). In the case of observational data, these values are often poorly constrained, so using the relative χ^2 values coupled with visual assessment of the data fit appears to be reasonable.

We also note that for the seven permanent stations for which we produce receiver function inversion/H-~~K~~κ

stacking results, five have estimates of Moho depth from previous receiver function studies. Clitheroe et al., (2000) estimated Moho depth at 49 km beneath CAN based on a non-linear inversion, which is ~10 km greater than the results we obtain for both NA inversion and H-κ stacking (see section 7.1 for further discussion of this discrepancy). Ford et al. (2010) determine Moho depth beneath stations MOO, TOO, TAU and YNG using H-κ ~~K~~-stacking ~~,~~and find values (compared to our H-κ ~~K~~ stacking results) of 33±3 km (33.0±1.2 km), 34±3 km (37.5±1.2 km), 32±3 km (33.5±1.9 km) and 33±2 km (37.3±~~1.2~~0.5 km) respectively. These are all within error, with the slight exception of station YNG, located in Young, on the western flanks of the Great Dividing Range, where we might expect the crust to be slightly thicker than average. Overall, however, these similarities suggest that our results are likely to be robust.

7 Discussion

For convenience, the seismic stations ~~were~~are separated into three groups (Fig. 2~~ and Table 2~~) based on tectonic setting~~s~~ and the results obtained. Stations YNG, CAN, CNB, MILA and BA13 are located in the Lachlan Fold Belt; stations BA02, BA11, BA19, BA20, TAU, MOO and TOO sit above the VanDieland microcontinental block; and stations BA07, BA08, BA09 and BA17 lie in the East Tasmania Terrane and Eastern Bass Strait (ETT+EB). Stations BA22 and BA24 lie to the west of VanDieland. This discussion focuses on crustal thickness, ~~and~~ the nature of the Moho and crustal velocity and velocity ratio variations from *H-κ* stacking and ~~the nature of the crust from *Vp/Vs*, Poisson's ratio and~~ the 1-D *S*-wave velocity models. Overall, the agreement between Moho depths obtained from the H-κ stacking results and NA-inversion is generally within error (Table 2), which makes a joint interpretation ~~more straight forwards~~more straight forward. Comparison is also made to other studies that have examined crustal seismic properties in southeast Australia, and we attempt to integrate our new findings with previous results from teleseismic tomography, SKS splitting and ambient noise tomography in order to better understand the crust and upper mantle structure and dynamics beneath this region.

7.1 Lateral variation of crustal thickness and nature of the Moho

The RF analysis clearly reveals the presence of lateral changes in crustal thickness that span mainland Australia through Bass Strait to Tasmania (Figures 6 and 10; in the latter case, RF depths from previous studies are also included for reference). The stations located in the Palaeozoic Lachlan Fold Belt reveal~~s~~ a generally thick crust that ranges ~~from 36.5 ± 4.4 to 39.1 ± 0.5 km~~between ~37 and ~~-~~40 km. ~~At station CAN, there is a disparity in crustal thickness obtained by the non-linear inversion method (~49 km) and *H-κ* stacking technique (39.1 ± 0.5 km). The reason appears to be that the *H-κ* stacking analysis assumes that the crust is a single layer with a velocity jump across the Moho, whereas the crust-mantle transition is actually gradual; hence it instead targets a shallower boundary that is not the Moho. Therefore, the deep crustal structure obtained at YNG, CAN and CNB is part of a broad velocity transition zone from crust to mantle. The crustal thickness and Moho transition zone beneath the Lachlan Orogen obtained by the nonlinear inversion method is consistent with previous refraction and RF studies~~ Although the Moho was picked as a velocity jump for stations YNG, CAN and CNB, the velocity nonetheless tends to continue to increase with depth below the discontinuity. This, coupled with the fact that Clitheroe et al. (2000) estimate the Moho to be almost 10 km deeper beneath CAN, is consistent with the presence of mafic underplating ~~(Shibutani et al., 1996; Clitheroe et al., 2000; Collins et al., 2003; Fontaine et al., 2013a,b). The crustal thickness variations and lack of a clear Moho at the base of the Lachlan Orogen crust may~~

be a consequence of mafic magmatic underplating (e.g. Drummond and Collins, 1986; Shibutani et al., 1996; Clitheroe et al., 2000), sourced from the ambient convecting mantle. The top and bottom of such a layer could feature a velocity jumpstep with depth; hence resulting in uncertainty in the true Moho depthand its internal structure is likely to be layered and/or gradational, hence resulting in uncertainty in the true Moho depth. This reinforces the opinion ofBased on deep crustal reflection profiling, Glen et al. (2002), who suggested that the deep Moho underlying the Lachlan Orogen results from magmatic underplating that added a thick Ordovician mafic layer at the base of the crust coupled with a thick sequence of Ordovician mafic rocks that can be found in the mid and lower crust. Finlayson et al. (2002) and Glen et al. (2002) also inferred the presence of underplating near CNB and CAN from seismic refraction data. Collins (2002) postulated that the underplating might have occurred in the back-arc region of a subduction zone due to pronounced adiabatic decompression melting in the asthenosphere. The seismic tomography model of Rawlinson et al. (2010, 2011) exhibits an increase in *P*-wavespeed at 50 km depth beneath CAN, CNB and YNG and the authors suggest that magmatic underplating may be the cause of the high velocity anomaly. A recent study by Davies et al. (2015) identified the longest continental hotspot track in the world (over 2000 km total length), which began in north Queensland at ~33 Ma, and propagated southward underneath the present daypresent-day Lachlan Fold Belt and Bass Strait. The magmatic underplating could therefore be a consequence of the passage of the continent above a mantle upwelling leading to a more diffuse crust-mantle transition zone. The thickened crust and a transitional Moho observed in the Lachlan Fold Belt are consistent with the proposed delamination models of Collins and Vernon (1994).

Strong lateral changes in crustal seismic structure (Figures 6 and 10) and/or composition beneath VanDieland appear to be a reflection of the region's complex tectonic history (Fig. 6 and 9). The thick crust (~37.5 ± 1.2 km) beneath the Selwyn Block (see Figure 1 for its location) – within the northern margin of VanDieland in southern Victoria – thins dramatically to ~26 km(to 30.5 ± 2.1 km) as it enters Bass Strait, increases to ~30 km beneath King Island (BA11), then thins to ~23 km beneath NW Tasmania, before increasing to ~33 km in southern Tasmania. yet in southern Tasmania, at stations TAU and MOO, the crust is thicker (33.5 ± 1.9 km). This is reflected in both the NA inversion and *H*-*κ* stacking depth estimates where a sharp Moho is observed beneath this region of the study area (Fig. 6 and 9). The Moho depth estimates from RFs at stations TAU and MOO (~34 km) is almost identical (~35 km) to that deducedThe results in southern Tasmania agree with those of by Korsch et al. (2002) from a seismic reflection profile adjacent to the two seismic stations TAU and MOO. In contrast, the Bass Strait portion of VanDieland appears to have a relatively thinner crust (~30 km). ThisThe thinner crust beneath Bass Strait and its margins may indicate thinning of the lithosphere associated with lithospheric stretchingbe a consequence of lithospheric thinning and/or delamination that resulted from tectonic events that occur post-formation of the Tasmanidesassociated with failed rifting that accompanied the break-up of Australia and Antarctica (Gaina et al., 1998).

Stations BA07, BA08, BA09 and BA17 (ETT+EB) collectively indicate crust of relative uniform thickness (~31-323 km, Figures 109a,b). Relative to western Bass Strait, the crust is slightly thickerthickens slightly in this part of the study area, which may suggest underplating associated with a Palaeozoic subduction system (e.g. Drummond and Collins, 1986; Gray and Foster, 2004). Furthermore, our results support the crustal thickness estimates of Tasmania from refraction and wide-angle reflection travel time tomography by Rawlinson et al.

~~(2001). They suggested that the thickening of the crust beneath central northern Tasmania is associated with the suturing of the West and East Tasmania Terranes during the Middle Devonian Tabberabberan Orogeny. The Moho depths we obtained at stations TAU, MOO, BA02 and BA11 which are located within their study area show significant overlap in crustal thickness estimates (Fig. S10 in supplementary material).~~

In general, our understanding of crustal thicknesses variations are limited by station separation, so it is difficult to determine whether smooth variations in thickness or step-like transitions explain the observations.

7.2 ~~Poisson's ratio,~~ *Vp/Vs* and bulk~~average~~ crustal composition

~~Poisson's ratio, which shares an inverse squared relationship to *Vp/Vs* (Eq. 2)~~ can constrain chemical composition and mineralogy more robustly than *P*- or *S*-wave velocity in isolation (Christensen and Fountain, 1975). We observe variations in ~~in Poisson's ratio (and hence *Vp/Vs*)~~ across the study region, which we can largely equate with variations in composition or melt. Studies in mineral physics and field observations show (1) a linear increase in Poisson's ratio with decreasing SiO_2 content in the continental crust (Christensen, 1996) and (2) partial melt is revealed~~depicted~~ by ~~an elevated Poisson's ratio (>0.30)~~elevated *Vp/Vs*, especially if the anomaly is localised to an intra-crustal layer (Owens and Zandt, 1997). ~~In terms of *Vp/Vs*, a~~A more felsic (SiO_2) composition in the lower crust is represented by a lower *Vp/Vs,* which reflects removal of an intermediate-mafic zone by delamination, whereas a more mafic lower crust is revealed~~depicted~~ by higher *Vp/Vs* (> 1.75) which may be due to underplated material (Pan and Niu, 2011). However, lower crustal delamination can also result in decompression melting, which can yield elevated *Vp/Vs*— (He et al., 2015). We interpret the variation of observed ~~Poisson's ratios (0.210–0.256)~~*Vp/Vs* in the southern Tasmanides to be a consequence of compositionally heterogeneous crust and localised partial melt that may likely be sourced from recent intraplate volcanism (Rawlinson et al., 2017).

Figure 6b shows the distribution of bulk *Vp/Vs* across the study area. The pattern of *Vp/Vs* ratios appears to delineate three distinct zones of crust. Beneath the Lachlan Orogen, values are ~1.75, which is consistent with the presence of a mafic lower crust, as suggested by a number of other studies (Drummond and Collins, 1986; Shibutani et al., 1996; Clitheroe et al., 2000; Finlayson et al., 2002). Beneath eastern Bass Strait, the *Vp/Vs* ratios are slightly lower, with BA07, BA08 and BA09 exhibiting values of 1.70, 1.70 and 1.71 respectively. These values are in agreement with constraints from seismic reflection and refraction studies (Finlayson et al., 2002; Collins et al., 2003) and may indicate a felsic to intermediate crustal composition. The geology of Flinders Island, which hosts both BA07 and BA08, is dominated by Devonian granites, which is consistent with this observation. Beneath VanDieland, *Vp/Vs* is highly variable, with the greatest contrast between BA11 (~1.65) and BA19/20 (~1.93), and BA19/20 and TOO (1.68). BA11 is located on King Island, which is characterised by Precambrian and Devonian granite outcrops, which may help explain the low *Vp/Vs*. The high *Vp/Vs* beneath BA19/20 is harder to explain, but could be caused by melt in the crust associated with the Newer Volcanics Province, which sits along the Cosgrove intraplate volcanic track, and last erupted only ~4.6 Ka (Rawlinson et al., 2017). The return to lower Vp/Vs beneath TOO over a relatively short distance (~100 km) is also difficult to explain, but we note that this region of Victoria is underlain by granite intrusions.

In summary, the crust beneath VanDieland exhibits the greatest lateral heterogeneity in *Vp/Vs*, which likely

reflects considerable variations in composition and the presence of melt. This can partially be explained by the tectonic history of the region, which includes failed rifting in Bass Strait accompanied by widespread magma intrusion and granite emplacement, and more recently, the passage of a plume (Rawlinson et al., 2017). Furthermore, Moore et al. (2015) used reflection transects and potential field data to infer that Vandieland is comprised of up to seven continental ribbon terranes that are bounded by major faults and suture zones, which were likely amalgamated by the end of the Proterozoic. Hence, considerable variations in composition and hence *Vp/Vs* ratio are to be expected.

~~Upon comparison with our Moho depth results (Fig. 6a and 9a,b), we find that areas of thick crust (Lachlan Fold Belt) do overlap with areas of higher *Vp/Vs* (1.70 ± 0.04 – 1.76 ± 0.04). This may strengthen the argument for mafic magmatic underplating sourced from an ambient convecting mantle (Glen et al., 2002). At MILA, BA13, CAN and CNB, the *Vp/Vs* values (1.70 ± 0.04–1.73 ± 0.06) are consistent with mafic granulite (Christensen and Fountain, 1975) which has been suggested to occur in the lower crust based on a wide-angle seismic line that cross-cuts the southern region of the Lachlan Orogen (Finlayson et al., 2002). At station YNG the *Vp/Vs* value of 1.76 ± 0.04 is consistent with biotite gneisses deduced from seismic reflection experiments carried out across the Junee-Narromine Volcanic Belt in the neighborhood of YNG (Direen et al., 2001).~~

~~The VanDieland *Vp/Vs* distribution is rather complex, hence we further divide this block into two separate groups: (1) West Tasmania Terrane (WTT); (2) and the Selwyn block. In the WTT, stations BA02, TAU, MOO (see Fig. 2 for the location) have a moderate *Vp/Vs* (1.69 ± 0.02–1.71 ± 0.04). The bulk *Vp/Vs* beneath BA02 (1.69 ± 0.02) supports a dominantly felsic crustal composition, which means that it is unlikely that the WTT has a mafic lower crust. A felsic crustal composition is at odds with the crustal composition required by the lower crustal flow model of Drummond and Collins (1986); Gray and Foster (2004). Our *Vp/Vs* measurement from the permanent GSN station TAU (1.70 ± 0.08), agrees well with *Vp/Vs* value at BA02 which implies a similar crustal composition. Station MOO adjacent to TAU exhibits a similar *Vp/Vs* value (1.71 ± 0.04) and together this may indicate that the crust is more or less homogeneous in this region. However, the slight variation in *Vp/Vs* values between station MOO and TAU may be associated with a slight change in bulk composition and the effects of heating following juxtaposition of western and eastern Tasmania during the Middle Devonian Tabberabberan Orogeny.~~

~~In Bass Strait and south central Victoria (underlain in part by the Selwyn Block), the abrupt variations in *Vp/Vs* values across stations BA11 and TOO help to underscore the region's complex tectonic evolution. Very few reliable *H-κ* stacking parameters were observed in this region: one on King Island (BA11) and the other adjacent to the NVP in south central Victoria. This is attributed to low signal quality/difficulty in identifying crustal multiples in this region (Chevrot and van der Hilst, 2000). The presence of a complex and compositionally variable Selwyn Block beneath the stations (Cayley et al., 2002), and melt-induced heating of the crust associated with the Quaternary NVP, may also be contributing factors. The *Vp/Vs* value at BA11 (1.65 ± 0.07) is the lowest in the study area which may imply a lower crustal delamination in Bass Strait, leaving a dominantly felsic crust (e.g. He et al., 2015; Bello et al., 2019b).~~

~~Station TOO located adjacent to the NVP exhibits a relatively low *Vp/Vs* (1.68 ± 0.04) that implies a more felsic composition, although mantle upwelling generated by the combined effects of a plume, SDU (shear driven upwelling) and EDC (edge driven convection) (Rawlinson et al., 2017) would likely yield melts of a mafic composition, so the low *Vp/Vs* may be caused by something else.~~

~~Despite the fact that crustal composition was possibly altered by recent deformational events that resulted from the break-up between Antarctica and Australia, similar *Vp/Vs* measurements are generally observed from the southern tip of Victoria through King Island to northwestern Tasmania. This suggests a tectonic relationship between northwest Tasmania and the Selwyn block and appears to support the presence of a coherent Precambrian microcontinental block (VanDieland) postulated by several studies in the preceding ~20 years (Cayley et al., 2002; Cayley, 2011; Moresi et al., 2014; Pilia et al., 2015a).~~

7.3 Moho depth comparison

Prior to this study, a variety of seismic methods have been used to constrain Moho depth in southeast Asia, including receiver functions, reflection profiling and wide-angle refection and refraction experiments. In an effort to combine the results from all of these studies into a single synthesis, Kennett et al., (2011) developed the AusMoho model. This included Moho depth estimates from over 11,000 km of reflection transects across the continent, numerous refraction studies, and 150 portable and temporary stations. Due to irregular sampling, the detail of this model is highly variable; for example, the region beneath Bass Strait is constrained by only five measurements, whereas the central Lachlan Fold Belt around Canberra (see Figure 1 for location) features relatively dense sampling at ~50 km intervals or less.

AusMoho includes previous receiver function results from Shibutani et al. (1996), Clitheroe et al. (2000), Fontaine et al. (2013a) and Tkalcic et al (2012), as well as reflection and refraction transects in Tasmania, parts of the Lachlan Orogen, and western Victoria. Figure 11 iIllustrates AusMoho for our study region, which exhibits large variations in Moho depth (from ~10 km to >50 km). These extremes are due to the presence of oceanic crust outboard of the passive margin of the Australian continent, and the root beneath the Southern Highlands, which represent the southern extension of the Great Dividing Range in New South Wales. Superimposed on Figure 11 are Moho depths from the four previous receiver function studies cited above, plus NA inversion and H-κ depth estimates from this study. As expected, the correlation between the previous RF results and AusMoho is generally good, since they were part of the dataset used to build this model. In places where they don't match, this can be attributed to the presence of seismic refraction or reflection lines which were also used to constrain AusMoho.

In general, the agreement between the results from this study and AusMoho is good, but there are exceptions. For instance, CAN, CNB, YNG and MILA tend to be somewhat shallower than AusMoho. However, this can be attributed to the likely presence of m~~M~~afic underplating alluded to earlier, which can effectively yield two options for the Moho transition due to an expected high (>1.85) *Vp/Vs* in the underplate layer (e.g. Cornwell et al., 2010). AusMoho Moho depths beneath BA07 and BA08 are considerably shallower than our estimates, which we attribute to a lack of data coverage in this region. Sizeable ~~discrepencies~~discrepancies also exist beneath BA02, BA19 and BA20; in the former case, the uncertainty in our H-κ stacking estimate is 5 km, which

may be a factor here. In the latter case, we also note that there is sparse data coverage southeast of Melbourne to constrain AusMoho, so it would appear that our new Moho depths are more likely to be correct. Overall, while there is good consistency between AusMoho and our new results, any updated version of AusMoho should incorporate the Moho depth estimates from this study.

Although AusMoho did make use of results from a 3-D wide-angle reflection and refraction survey of Tasmania (offshore shots and on-shore stations), it only used a few sample points for the final Moho model (Kennett et al., 2011), and therefore the resolution of AusMoho is considerably less than the Moho model produced by Rawlinson et al. (2001). Consequently, we plot our three RF results on top of this model in Supplementary Figure S9. The agreement between the Moho model and RF depths beneath MOO and TAU is good, but RF estimates beneath BA02 are shallower than the Moho model by about 4 km. However, this is within the margin of error for the H-κ stacking result.

7.4 Synthesis

In this final section, we present a synthesis of results for southeast Australia that are based on: (1) our new receiver function results; (2) teleseismic SKS splitting results from Bello et al. (2019a); (3) teleseismic tomography undertaken by Bello et al. (2019b); (4) ambient noise crustal imaging results from Young et al. (2013); and (5) AusMoho (Kennett et al., 2011). This synthesis is encapsulated in the plot shown in Figure 12, which is a representative transect through the Lachlan Orogen south through Bass Strait and into Tasmania. Moho depths are taken from AusMoho, and refined where additional information is available from our new RF results; crustal ~~PH~~P-wave velocity is taken from the ambient noise results (following conversion from *S*-wave velocity – see Bello et al, 2019b for more details); and mantle *P*-wave velocities are taken from Bello et al, (2019b). Arrows are based on interpreted mantle flow patterns undertaken as part of the shear wave splitting study. This previous study used approximately the same temporary and broadband station network that was used in the current study, and found that beneath the Lachlan Orogen, fast axis orientations of anisotropy were aligned with contemporary plate motion (NNE), but beneath Bass Strait, a radial pattern was observed that is consistent with an upwelling mantle that impinges on the lithosphere and spreads out in all directions. Interestingly, the location of this phenomenon corresponds approximately to the predicted location of the Cosgrove hotspot track source (Davies et al., 2015), and may be caused by an upwelling mantle plume. Thus, the low velocities in the upper mantle beneath Bass Strait may be due to elevated temperatures and melt, although it is not straightforward to explain the higher velocities below 200 km depth in this context.

The thicker Moho boundary beneath the Lachlan Orogen (Figure 12) reflects the likely presence of underplating, which makes the base of the crust harder to discern seismically. However, the crust is clearly thicker here than beneath Bass Strait or Tasmania. Moho depth beneath the northern part of the Figure 12 is not constrained by our RF results, but according to AusMoho, it is relatively flat, which is consistent with Precambrian crust, and there is a faster mantle lithosphere. The strong variations in crustal velocity beneath Bass Strait can be attributed to failed rifting resulting in the formation of thick (>10 km) sedimentary basins and elevated temperatures (lower velocities), and intrusion of mafic rich material into the lower and mid crust (higher velocities).

8 Conclusions

We used *H-κ* stacking of teleseismic RFs to determine crustal thickness and *Vp/Vs* ~~ratios; we also~~ratio and generate 1-D *S*-wave velocity profiles of the crust from ~~1-D~~ RF inversion in order to investigate the internal crustal velocity structure beneath the southern Tasmanides in southeast Australia. ~~We were able to verify the presence of several crustal structures imaged by previous studies (Clitheroe et al., 2000; Finlayson et al., 2002; Glen et al., 2002; Reading et al., 2011; Fontaine et al., 2013a,b) where there is overlap and we have also been able to provide new estimates of crustal thickness and composition. We have also been able to shed fresh light on the different tectonic blocks that constitute southeast Australia. The major conclusions are as follows:~~ Our main findings are summarised below.

- The thick crust and broad crust-mantle transition beneath the Lachlan Fold Belt may be caused by magmatic underplating of mafic materials beneath the crust, which is consistent with a ~~relatively high Poisson's ratio (0.262 ± 0.014)~~n elevated *Vp/Vs* ratio (relative to ak135) of ~1.73. Thicker crust is also to be expected from the elevated topography ~~beneath~~of the eastern Lachlan Fold Belt.

- The crustal structure is complex beneath~~in~~ VanDieland. It thins considerably from the northern tip of the microcontinent (~37 km) into Bass Strait (~26 km) and northern Tasmania (~23 km), yet in southern Tasmania the crust is somewhat thicker (~33~~.5 ± 1.9 km~~ km) compared to Bass Strait. This may in part be due to the complex origins of the microcontinent, which appears to be comprised of multiple Precambrian continental ribbons, but is also likely due to failed rifting in Bass Strait before and during the separation of Australia and Antarctica. This resulted in lithospheric stretching/delamination, magmatic intrusion, and the deposition of thick sedimentary sequences. Recent intraplate volcanism and the possible progression of a mantle plume beneath Vandieland in the last few thousand years may also have produced compositional heterogeneity and melt in the crust. Such events are likely to contribute significantly to variations in crustal thickness and the pronounced changes in *Vp/Vs* that we observe. ~~This scenario may be attributed to the break-up of Antarctica and Australia and the opening of the Tasman Sea which formed three failed rift basins that contain thick piles of sedimentary rocks (Gaina et al., 1998). The thinner crust beneath Bass Strait may indicate that the thinning of the lithosphere is associated with processes such as delamination and/or stretching of the lithosphere during the break-up of the two continents.~~

- Stations within the~~at~~ ETT+EB collectively indicate crust of uniform thickness (~31-32~~3~~ km) and uniform *Vp/Vs* (~1.70) ~~and an intermediate Moho transition which possibly reflects underplating associated with a Palaeozoic subduction system.~~, which clearly distinguishes it from Vandieland. This region of the crust likely represents a southern continuation of the Lachlan Orogen, and therefore is underpinned by crust of oceanic origin.

- ~~It is clear that the nature of velocity anomalies differ between stations on mainland Australia and Tasmania. This highlights contrasting lithospheric structure across Bass Strait (~ 40°S) with thin lithosphere to the south and thick lithosphere to the north. This sharp transition of lithospheric~~

~~thickness is in agreement with previous results (Clitheroe et al., 2000) and corresponds to changes in fast *S*-wave polarization directions from primarily northeast-southwest orientations in the north to nearly northwest-southeast directions in the south (Heintz and Kennett, 2005; Pilia et al., 2016; Bello et al., 2019a).~~ Comparison of our new Moho depth results with the AusMoho model reveals an overall consistency, although at some of our station locations where AusMoho has few constraints, there are noticeable differences, such as southern Victoria and beneath Flinders Island. The discrepancies beneath the Lachlan Orogen are attributed to the presence of underplated mafic material, which can obfuscate the location of the Moho.

- A synthesis of our new RF results with ~~prexisting~~pre-existing teleseismic tomography, shear wave splitting and ambient noise studies reveals a complex lithosphere that has clearly been impacted by orogeny (thickened crust), failed rifting beneath Bass Strait (thinned crust and complex crustal velocities), and recent intraplate volcanism (high *Vp/Vs* ratios and a radial pattern of fast anisotropy patterns above a presumed zone of mantle upwelling).

~~Results from this study advance our understanding of the nature and composition of different tectonic blocks that constitute the geology of the southern Tasmanides. These results will also be important for helping to understand the results from other comparable seismic imaging studies and the interpretation of tectonic processes on a wider scale.~~

9 Data availability

Dataset available at 10.6084/m9.figshare.12233723

10 Author contributions

M.B. performed the data analysis and wrote the draft manuscript. N.R and D.C. guided the study and assisted in interpretation. M.B., D.C. and N.R. discussed the results and revised the manuscript. A.R. and O.L. revised the manuscript and assisted with the interpretation.

11 Competing Interests: The authors declare no competing interests.

12 Acknowledgments

The work in this paper was performed as part of a PhD study and has been jointly funded by Abubakar Tafawa Balewa University (ATBU), Bauchi, Nigeria and the University of Aberdeen, UK. The authors acknowledge the efforts of staff, students and fieldwork technicians from the Australian National University and University of Tasmania, who deployed the temporary BASS array used in this study. We also thank Qi Li and Armando Arcidiaco for their efforts in BASS data pre-processing and archiving. Australian Research Council Grant LP110100256 supported the BASS deployment. We are grateful to IRIS and Geoscience Australia for providing data from several stations in mainland Australia and Tasmania. Figure 1 was made using Inkscape software (Harrington, et. al., 2005) and Figures 2, 3, 6 and 9 were produced using the Generic Mapping Tools (Wessel et al., 2013).

References

Amante, C. and Eakins, B. W.: ETOPO1 1 Arc-Minute Global Relief Model: Procedures, data sources and analysis, NOAA technical memorandum NESDIS NGDC-24, 19pp, 2009.

Ammon, C. J.: The isolation of receiver effects from teleseismic P waveforms. Bull. Seis. Soc. Ame., 81, 2504–2510, 1991.

Ammon, C. J., Randall, G., and Zandt, G.: On the nonuniqueness of receiver function inversions. J. Geophys. Res., 95, 15 303–15 318, 1990.

Arroucau, P., Rawlinson, N., and Sambridge, M.: New insight into Cainozoic sedimentary basins and Palaeozoic suture zones in southeast Australia from ambient noise surface wave tomography. Geophys. Res. Lett., 37, http://dx.doi.org/10.1029/2009GL041974, 2010.

Bannister, S., Yu, J., Leitner, B., and Kennett, B. L. N.: Variations in crustal structure across the transition from West to East Antarctica, Southern Victoria Land, Geophys. J. Int., 155, 870–884, 2003.

Bello, M., Cornwell, D. G., Rawlinson, N., and Reading, A. M.: Insights into the structure and dynamics of the upper mantle beneath Bass Strait, southeast Australia, using shear wave splitting, Phys. Earth Planet. Inter., 289, 45–62, https://doi.org/10.1016/j.pepi.2019.02. 002, 2019a.

Bello, M., Rawlinson, N., Cornwell, D. G., Crowder, E., Salmon, M., and Reading, A. M.: Structure of the crust and upper mantle beneath Bass Strait, southeast Australia, from teleseismic body wave tomography, Phys. Earth Planet. Inter., 294, https://doi.org/10.1016/j.pepi. 2019.106276, 2019b.

Berry, R. F., Steele, D. A., and Maffre, S.: Proterozoic metamorphism in Tasmania: implications for tectonic reconstructions, Prec. Res., 166, 387–396. https://doi.org/10.1016/j. precamres.2007.05.004, 2008.

Bodin, T., Salmon, M., Kennett, B. L. N., and Sambridge, M.: Probabilistic surface reconstruction from multiple datasets: an example for the Australian Moho, J. Geophys. Res.: Solid Earth, 117, http://dx.doi.org/10.1029/2012JB009547, 2012a.

Bodin, T., Sambridge, M., Rawlinson, N., and Arroucau, P.: Transdimensional tomography with unknown data noise, Geophys. J. Int., 189, 1536–1556, 2012b.

Boger, S. and Miller, J.: Terminal suturing of Gondwana and the onset of the Ross Delamerian Orogeny: the cause and effect of an Early Cambrian reconfiguration of plate motions, Earth Planet. Sci. Lett., 219, 35–48, 2004.

Calvert, C. R. and Walter, M. R.: The Late Neoproterozoic Grassy Group of King Island, Tasmania: correlation and palaeogeographic significance, Precam. Res., 100, 299–312, 2000.

Cawood, P. A.: Terra Australis Orogen: Rodinia breakup and development of the Pacific and Iapetus margins of Gondwana during the Neoproterozoic and Palaeozoic. Earth-Science Reviews, 69, 249–279, http://dx.doi.org/10.1016/j.earscirev.2004.09.001, 2005.

Cayley, R.: Exotic crustal block accretion to the eastern Gondwanaland margin in the Late Cambrian Tasmania, the Selwyn Block, and implications for the Cambrian–Silurian evolution of the Ross, Delamerian, and Lachlan orogens. Gond. Res., 19, 628–649. http://dx.doi.org/10. 1016/j.gr.2010.11.013, 2011a.

Cayley, R., Korsch, R. J., Moore, D. H., Costelloe, R. D., Nakamura, A., Willman, C. E., Rawlin, T. J., Morand, V. J., Skladzien, P. B., and O'Shea, P. J.: Crustal architecture of central Victoria: results from the 2006 deep crustal reflection seismic survey, Aust. J. Earth Sci., 59, 113–156, 2011b.

737 ~~Cayley, R., Taylor, D. H., VandenBerg, A. H. M., and Moore, D. H.: Proterozoic–Early Palaeozoic rocks and~~
738 ~~the Tyennan Orogeny in central Victoria: the Selwyn Block and its tectonic implications, Aust. J. Earth Sci.,~~
739 ~~49, 225-254, 2002.~~

740 Chen, Y., Niu, F., Liu, R., Huang, Z., Tkalčić, H., Sun, L., and Chan, W.: Crustal structure beneath China from
741 receiver function analysis, J. Geophys. Res., 49(B033067), 2010.

742 Chevrot, S. and van der Hilst, R. D.: The Poisson ratio of the Australian crust: Geological and Geophysical
743 implications, Earth Planet. Sci. Lett., 183,121–132, 2000.

744 Christensen, N. I.: Poisson's ratio and crustal seismology, J. Geophys. Res., 101, 3139–3156, 1996.

745 Christensen, N. I. and Fountain, D. M.: Constitution of the lower continental crust based on experimental studies
746 of seismic velocities in granulite, Geol. Soc. Ame. Bull., 86, 227–236, 1975.

747 Clitheroe, G., Gudmundsson, O., and Kennett, B.: The crustal thickness of Australia, J. Geophys. Res., 105, 13
748 697–13 713, 2000.

749 Collins, C. D. N.: The nature of crust–mantle boundary under Australia from seismic evidence, In: Drummond
750 B. J. ed. The Australian lithosphere, Geol. Soc. Aust. Spec. Pub., 17, 67–80, 1991.

751 Collins, C. D. N., Drummond, B. J., and Nicoll, M. G.: Crustal thickness patterns in the Australian continent,
752 Geol. Soc. Ame. Spec. Papers, 372, 121–128, 2003.

753 Collins, W. J.: Nature of extensional accretionary origins, Tectonics, 21, 1024–1036, 2002.

754 Collins, W. J. and Vernon, R. H.: A rift–drift–delamination model of continental evolution: Palaeozoic tectonic
755 development of eastern Australia, Tectonophysics, 2(35), 1994.

756 Coney, P. J.: Plate tectonics and the Precambrian Phanerozoic evolution of Australia, PACRIM '95, Aust. Inst.
757 Mining and Metallurgy, pages 145–150, 1995.

758 Coney, P. J., Edwards, A., Hine, R., Morrison, F., and Windrim, D.: The regional tectonics of the Tasman
759 orogenic system, eastern Australia, J. Struct. Geol., 12(5/6), 519–543, 1990.

760 Cornwell, D. G., P. K. H. Maguire, R. W. England, and G. W. Stuart (2010), Imaging detailed crustal structure
761 and magmatic intrusion across the Ethiopian Rift using a dense linear broadband array, *Geochem. Geophys.*
762 *Geosyst.*, **11**, Q0AB03, doi:10.1029/2009GC002637.

763 Crowder, E., Rawlinson, N., Pilia, S., Cornwell, D. G., and Reading, A. M.: Transdimensional ambient noise
764 tomography of Bass Strait, southeast Australia, reveals the sedimentary basin and deep crustal structure
765 beneath a failed continental rift, Geophys. J. Int., 217, 970–987, 2019.

766 Davies, D. R., Rawlinson, N., Iaffaldano, N., and Campbell, I. H.: Lithospheric controls on magma composition
767 along Earth's longest continental hotspot track, Nature, 525, 511–514, 2015.

768 ~~Direen, N. G., Lyons, P., Korsch, R. J., and Glen, R. A.: Integrated geophysical appraisal of crustal architecture~~
769 ~~in the Eastern Lachlan Orogen, Explo. Geophys., 32, 252–262, 2001.~~

770 Drummond, B. J. and Collins, C. D. N.: Seismic evidence for underplating of the lower continental crust of
771 Australia, Earth Planet. Sci. Lett., 79, 361–372, 1986.

772 Drummond, B. J., Lyons, P., Goleby, B., and Jones, L.: Constraining models of the tectonic setting of the giant
773 Olympic Dam iron-oxide-copper-gold deposit, south Australia, using deep seismic reflection data,
774 Tectonophysics, 420, 91–103, 2006.

775 Eagar, K. C. and Fouch, M. J.: FuncLab: A MATLAB interactive toolbox for handling receiver function
776 datasets, Seismo. Res. Lett., https://doi.org/10.1785/gssrl.83.3.596, 2012.

Finlayson, D. M., Collins, C. D. N., and Denham, D.: Crustal structure under the Lachlan Fold Belt, southeastern Australia, Phys. Earth Planet. Int., 21, 321–342, 1980.

Finlayson, D. M., Korsch, R. J., Glen, R. A., Leven, J. H., and Johnstone, D. W.: Seismic imaging and crustal architecture across the Lachlan transverse zone, a crosscutting feature of eastern Australia, Aust. J. Earth Sci., 49, 311–321, 2002.

Fishwick, S. and Rawlinson, N.: 3–D structure of the Australian lithosphere from evolving seismic datasets, Aust. J. Earth Sci., 59, 809–826, 2012.

Foden, J., Elburg, M. A., Dougherty-Page, J., and Burtt, A.: The timing and duration of the Delamerian Orogeny: correlation with the Ross Orogen and implications for Gondwana assembly, J. Geology, 114, 189–210, 2006.

Fontaine, F. R., Tkalčić, H., and Kennett, B. L. N.: Crustal complexity in the Lachlan Orogen revealed from teleseismic receiver functions, Aust. J. Earth Sci., 60, 413–430, 2013a.

Fontaine, F. R., Tkalčić, H., and Kennett, B. L. N.: Imaging crustal structure variation across southeastern Australia, Tectonophysics, 582, 112–125, 2013b.

Foster, D. A. and Gray, D. R.: Evolution and structure of the Lachlan Fold Belt (Orogen) of eastern Australia, Annu. Rev. Earth Planet. Sci., 28, 47–80, 2000.

Gaina, C., Müller, D., Royer, J. Y., Stock, J., Hardebeck, J., and Symonds, P.: The tectonic history of the Tasman Sea, a puzzle with 13 pieces, J. Geophys. Res., 103,12,413–12,433,1998.

Gibson, G. M., Morse, M. P., Ireland, T. R., and Nayak, G. K.: Arc-continent collision and orogenesis in western Tasmanides: insights from reactivated basement structures and formation of an ocean-continent transform boundary off western Tasmania, Gondwana Res., 19, 608–627, 2011.

Glen, R. A.: The Tasmanides of Eastern Australia. In: Vaughan, A. P. M., Leat, P. T., Pankhurst, R. J. (Eds.), Terrane Processes at the Margins of Gondwana, Geological Society, pages 23–96, 2005.

Glen, R. A.: Refining accretionary orogen models for the Tasmanides of eastern Australia, Aust. J. Earth Sci., 60, 315–370, 2013.

Glen, R. A., Korsch, R. J., Direen, N. G., Jones, L. E. A., Johnstone, D. W., Lawrie, K. C., Finlayson, D. M., and Shaw, R. D.: Crustal structure of the Ordovician Macquarie Arc, eastern Lachlan Orogen, based on seismic–reflection profiling, Aust. J. Earth Sci., 49, 323–348, 2002.

Glen, R. A., Percival, I. G., and Quinn, C. D.: Ordovician continental margin terranes in the Lachlan Orogen, Australia: implications for tectonics in an accretionary orogen along the east Gondwana margin, Tectonics, 28, https://doi.org/:10.1029/2009TC002446, 2009.

Goldstein, P., Dodge, D., Firpo, M., and Minner, L.: SAC2000: Signal processing and analysis tools for seismologists and engineers. Lee, W. H. K. and Kanamori, H. and Jennings, P. C. and Kisslinger, C. (Eds.). In IASPEI International Handbook of Earthquake and Engineering Seismology, Academic Press, London, 2003.

Gouveia, W. P. and Scales, J. A.: Bayesian seismic waveform inversion: Parameter estimation and uncertainty analysis, J. Geophys. Res., 103, 2759–2779, 1998.

Gray, D. R. and Foster, D. A.: Tectonic evolution of the Lachlan Orogen, southeastern Australia: historical review, data synthesis and modern perspectives, Aust. J. Earth Sci., 51, 773– 817, 2004.

Gunn, P. J., Maidment, D. W., and Milligan, P.: Interpreting aeromagnetic data in areas of limited outcrop, AGSO J. Aust. Geol. Geophys., 17, 175–185, 1997.

Harrington, B. et al (2004-2005). Inkscape. http://www.inkscape.org/.

Haskell, N. A.: The dispersion of surface waves in multilayered media, Bulletin of the Seismological Society America, 43, 1734, http://dx.doi.org/10.1038/physci245109a0, 1953.

He, C. S., Santosh, M., Dong, S. W., and Wang, S. C.: Crustal thickning and uplift of the Tibetan Plateau inferred from receiver function analysis, J. Asian Earth Sci., 99,112–124, 2015.

Heintz, M. and Kennett, B. L. N.: Continental scale shear wave splitting analysis: Investigation of seismic anisotropy underneath the Australian continent, Earth Planet. Sci. Lett., 236, 106–119, 2005.

Kennett, B. L. N, Engdhal, E. R., and Buland, R.: Constraints on seismic velocities in the earth from travel times. Geophys. J. Int., 125, 228-248, 1995.

Kennett, B. L. N. and Furumura, T.: Stochastic waveguide in the lithosphere: Indonesian subduction zone to Australian craton, Geophys. J. Int., 172, 363–382, 2008.

Kennett, B. L. N., Salmon, M., Saygin, E., and Group, A.: AusMoho: the variation of Moho depth in Australia, Geophys. J. Int., 187, 946–958, 2011.

Korsch, R. J., Barton, T. J., Gray, D. R., Owen, A. J., and Foster, D. A.: Geological interpretation of a deep seismic reflection transect across the boundary between the Delamerian and Lachlan Orogens, in the vicinity of the Grampians, western Victoria, Aust. J. Earth Sci., 49, 1057–1075, http://dx.doi.org/10.1046/j.1440-0952.2002.00963.x, 2002.

Langston, C. A.: Structure under Mount Rainier, Washington, inferred from teleseismic body waves, J. Geophys. Res., 84, 4749–4762, https://doi.org/10.1071/EG994019, 1979.

Li, Z. X., Baillie, P. W., and Powell, C. M.: Relationship between northwestern Tasmania and East Gondwanaland in the Late Cambrian/Early Ordovician Paleomagnetic evidence, Tectonics, 16, 161–171, http://dx.doi.org/10.1029/96TC02729, 1997.

Ligorria, J. P. and Ammon, C. J.: Iterative deconvolution and receiver function estimation, Bull. Seism. Soc. Ame., 89, 1395–1400, 1999.

~~Mavko, M.: Velocity and attenuation in partially molten rocks, J. Geophys. Res., 85, 5173–5189, https://doi.org/10.1029/JB085iB10p05173, 1980.~~

Moore, D., Betts, P. G., and Hall, M.: Fragmented Tasmania: the transition from Rodinia to Gondwana, Aust. J. Earth Sci., 62, 1–35, 2015.

Moore, D. H., Betts, P. G., and Hall, M.: Constraining the VanDieland microcontinent at the edge of East Gondwana, Australia, Tectonophysics, 687, 158–179, 2016.

Moresi, L., Betts, P. G., Miller, M. S., and Cayley, R. A.: Dynamics of continental accretion, Nature, 508, 245–248, 2014.

Morse, M., Gibson, G., and Mitchell, C.: Basement constraints on offshore basin architecture as determined by new aeromagnetic data acquired over Bass Strait and western margin of Tasmania, ASEG Extended Abstracts 2009, pages 1–9, http://dx.doi.org/10.1071/ASEG2009ab042, 2009.

~~O'Connel, R. J. and Budiansky, B.: Seismic velocities in dry and saturated cracked solids, J. Geophys. Res., 79, 5412-5426, 1974.~~

Owens, T. J., Taylor, S. R., and Zandt, G.: Crustal structure at regional seismic test network stations determined from inversion of broadband teleseismic P waveforms, Bull. Seismo. Soc. Ame., 77, 631–632, 1987.

Owens, T. J. and Zandt, G.: Implications of crustal property with variations for models of Tibetan Plateau evolution, Nature, 387, 37–43, 1997.

Pan, S. Z. and Niu, F. L.: Large contrasts in crustal structure and composition between the Ordos plateau and the

NE Tibetan plateau from receiver function analysis, Earth Plan. Sci. Lett., 303, 291–298, 2011.

Pilia, S., Arroucau, P., Rawlinson, N., Reading, A. M., and Cayley, R. A.: Inherited crustal deformation along the East Gondwana margin revealed by seismic anisotropy tomography, Geophys. Res. Lett., 43(23), 12082–12090, https://doi.org/10.1002/2016GL071201, 2016.

Pilia, S., Rawlinson, N., Cayley, R. A., Musgrave, R., Reading, A. M., Direen, N. G., and Young, M. K.: Evidence of micro–continent entrainment during crustal accretion, Sci. Rep., 5, http://dx.doi.org/10.1038/srep/08218, 2015a.

Pilia, S., Rawlinson, N., Green, N. G., Reading, A. M., Cayley, R., Pryer, L., Arroucau, P., and Duffet, M.: Linking mainland Australia and Tasmania using ambient seismic noise tomography: Implications for the tectonic evolution of the east Gondwana margin, Gond. Res., 28, 1212–1227, 2015b.

Porritt, S. W. and Miller, M. S.: Updates to FuncLab, a Matlab based GUI for handling receiver functions, Computers and Geosciences, 111, 260–271, https://doi.org/10.1016/j. cageo.2017.11.022, 2018.

Rawlinson, N., Davies, D. R., and Pilia, S.: The mechanisms underpinning Cenozoic intraplate volcanism in eastern Australia, Insights from seismic tomography and geodynamic modeling, Geophys. Res. Lett., 44(19), 9,681–9,690, 2017.

Rawlinson, N., Housman, G. A., Collins, C. D. N., and Drummond, B. J.: New evidence of Tasmania's tectonic history from a novel seismic experiment, Geophys. Res. Lett., 28, 3337–3340, 2001.

Rawlinson, N. and Kennett, B.: Teleseismic tomography of the upper mantle beneath the southern Lachlan Orogen, Australia, Phys. Earth Planet. Inter., 167, 84–97, http://dx.doi.org/ 10.1016/j.pepi2008.02.07, 2008.

Rawlinson, N., Kennett, B., Vanacore, E., Glen, R., and Fishwick, S.: The structure of the upper mantle beneath the Delamerian and Lachlan orogens from simultaneous inversion of multiple teleseismic datasets, Gond. Res., 19, 788–799, 2011.

Rawlinson, N., Kennett, B. L. N., Salmon, M., and Glen, R. A.: Origin of lateral heterogeneities in the upper mantle beneath Southeast Australia from seismic tomography, Khan, A., and Deschamps, F. (Eds.), In The Earth's Heterogeneous Mantle: A Geophysical, Geodynamical and Geochemical Perspective, pages 47–78, Springer Geophysics, Springer, 2015.

Rawlinson, N., Pilia, S., Young, M., Salmon, M., and Yang, Y.: Crust and upper mantle structure beneath southeast Australia from ambient noise and teleseismic tomography, Tectonophysics, 689, 143–156, http://dx.doi.org/10.1016/j.tecto.2015.11.034, 2016.

Rawlinson, N., Pozgay, S., and Fishwick, S.: Seismic tomography: a window into deep Earth, Phys. Earth Planet. Inter., 178, 101–135, 2010.

Rawlinson, N. and Urvoy, M.: Simultaneous inversion of active and passive source datasets for 3–D seismic structure with application to Tasmania, Geophys. Res. Lett., 33, 2006.

~~Reading, A. M., Tkalčić, H., Kennett, B. L. N., Johnson, S. P., and Sheppard, S.: Seismic structure of the crust and uppermost mantle of the Capricon and Paterson Orogens and adjacent cratons, Western Australia, from passive seismic transects, Prec. Res., 196–197, 295–308, 2011.~~

Sambridge, M. S.: Geophysical inversion with a neighbourhood algorithm – I. Searching a parameter space, Geophys. J. Int., 138, 479–494, 1999a.

Sambridge, M. S.: Geophysical inversion with a neighbourhood algorithm -II. Appraising the ensemble, Geophys. J. Int., 138, 479–494, 1999b.

Saygin, E. and Kennett, B. L. N.: Ambient seismic noise tomography of Australian continent, Tectonophysics, 481, 116–125, http://dx.doi.org/10.1016/j.tecto.2008.11.013, 2010.

Shibutani, T., Sambridge, M. S., and Kennett, B. L. N.: Genetic algorithm inversion for receiver functions with application to crust and uppermost mantle structure beneath Eastern Australia, Geophys. Res. Lett., 23,1826–1832, 1996.

Spaggiari, C. V., Gray, D. R., and Foster, D. A.: Lachlan Orogen subduction–accretion systematics revisited, Aust. J. of Earth Sci., 51, 549–553, 2004.

Spaggiari, C. V., Gray, D. R., Foster, D. A., and McKnight, S.: Evolution of the boundary between the western and central Lachlan Orogen: implications for Tasmanide tectonics, Aust. J. Earth Sci., 50, 725–749, 2003.

Teasdale, J., Pryer, L., Stuart-Smith, P., Romine, K., Etheridge, M., Loutit, T., and Kyan, D.: Structural framework and basin evolution of Australia's Southern Margin, APPEA J. Australian Petroleum Production and Exploration Association, 43, 13–38, https://doi.org/10. 1785/0120030123, 2003.

Thomson, W. T.: Transmission of elastic waves through a stratified solid, J. of App. Phys., 21, 89-93, 1950.

Tkalčić, H., Chen, Y., Liu, R., Huang, H., Sun, L., and Chan, W.: Multi–step modelling of teleseismic receiver functions combined with constraints from seismic tomography: Crustal structure beneath southeast China, Geophys. J. Int., 187, 303–326, 2011.

Tkalčić, H., Rawlinson, N., Arroucau, P., and Kumar, A.: Multistep modelling of receiver-based seismic and ambient noise data from WOMBAT array: crustal structure beneath southeast Australia, Geophys. J. Int., 189, 1681–1700, https://doi.org/10.1111/j.1365-246X.2012.05442, 2012.

Wessel, P., Smith, W. H., Scharroo, R., Louis, J., and Wobbe, F.: Generic mapping tools: improved version released, EOS Trans. Am. Geophys. Union, 94, 409-420, 2013.

~~White, L., Gibson, G., and Lister, G.: A reassessment of paleogeographic reconstructions of eastern Gondwana: bringing geology back into the equation, Gond. Res., 24, 984–998, http://dx.doi.org/10.1016/j.gr.2013.06.00, 2013.~~

Young, M. K., Cayley, R. A., McLean, M. A., Rawlinson, N., Arroucau, P., and Salmon, M.: Crustal structure of the east Gondwana margin in southeast Australia revealed by transdimensional ambient seismic noise tomography, Geophys. Res. Lett., 40, 4266–4271, 2013.

Young, M. K., Rawlinson, N., Arroucau, P., Reading, A., and Tkalčić, H.: High–frequency ambient noise tomography of southeast Australia: new constraints on Tasmania's tectonic past, Geophys. Res. Lett., 38, http://dx.doi.org/10.1029/2011GL047971, 2011.

Young, N., Tkalčić, H., Rawlinson, N., and Reading, A. M.: Full waveform moment tensor inversion in a low seismicity region using multiple teleseismic datasets and ambient noise: application to the 2007 Shark Bay, Western Australia, Earthquake. Geophys. J. Int., 188,1303–1321, https://doi.org/10.1111/j.1365-246X.2011.05326, 2012.

Zhu, L. and Kanamori, H.: Moho depth variation in southern California from teleseismic receiver functions, J. Geophys. Res., 105, 2969–2980, 2000.

Table 1: Model parameter bounds used in the Neighbourhood Algorithm receiver function inversion. V_s^{upper} and V_s^{lower} represent the S-velocity at the top and bottom of a layer respectively. V_p/V_s represents P and S wave velocity ratio within a layer.

Layer	Thickness (m)	V_s^{upper} (km/s)	V_s^{lower} (km/s)	V_p/V_s
Sediment	0-2	0.5-1.5	0.5-1.5	2.00-3.00
Basement	0-3	1.8-2.8	1.8-2.8	1.65-2.00
Upper crust	3-20	3.0-3.8	3.0-3.9	1.65-1.80
Middle crust	4-20	3.4-4.3	3.4-4.4	1.65-1.80
Lower crust	5-15	3.5-4.8	3.6-4.9	1.65-1.80
Mantle	5-20	4.0-5.0	4.0-5.0	1.70-1.90

Table 2: Summary of H-κ stacking and NA inversion results for the current study.

Basic station information					Results				
Type	Station name	Lon (°)	Lat (°)	No of RFs	Moho Depth (km) (H-K stacking)	Bulk Vp/Vs (H-K stacking)	Moho Depth (km) (NA inversion)	Quality (NA inversion)	Moho type (NA inversion)
Temporary stations	BA02	145.20	-40.95	9	23.2±5.0	1.83±0.31	-	Moderate	Not evident
	BA03	145.84	-41.20	8	-	-	-	Moderate	Not evident
	BA07	148.31	-40.43	6	32.5±0.1	1.70±0.02	28	Good	Sharp
	BA08	147.97	-39.77	8	31.9±0.1	1.70±0.07	-	Poor	-
	BA09	147.32	-39.47	8	32.8±1.7	1.71±0.07	32	Good	Sharp
	BA11	143.98	-39.64	12	30.5±2.1	1.65±0.07	-	-	-
	BA13	148.83	-37.63	24	37.7±2.9	1.74±0.10	40	Good	Sharp
	BA17	146.33	-39.04	20	30.9±2.5	1.76±0.10	29	Good	Broad
	BA18	146.14	-38.02	3	-	-	38	Good	Sharp
	BA19	145.69	-38.57	20	25.5±2.4	1.93±0.14	-	Good	Not evident
	BA20	144.92	-38.42	30	26.3±1.6	1.93±0.12	29	Good	Sharp
	BA22	143.61	-37.99	5	-	-	29	Poor	Sharp
	BA24	142.54	-38.26	4	-	-	33	Poor	Sharp
Permanent stations	TAU	147.32	-42.91	41	33.5±1.9	1.70±0.08	33	Poor	Intermediate
	MOO	147.19	-42.44	58	33.0±1.2	1.71±0.04	34	Good	Sharp
	TOO	145.59	-37.57	276	37.5±1.2	1.68±0.04	36	Good	Sharp
	YNG	148.40	-34.20	178	37.3±0.5	1.76±0.04	35	Good	Sharp
	CAN	149.00	-35.32	402	39.1±0.5	1.73±0.02	40	Good	Sharp
	CNB	149.36	-35.32	155	38.5±1.1	1.70±0.04	39	Good	Broad
	MILA	149.16	-37.05	4	37.6±2.1	1.73±0.06	-	-	-

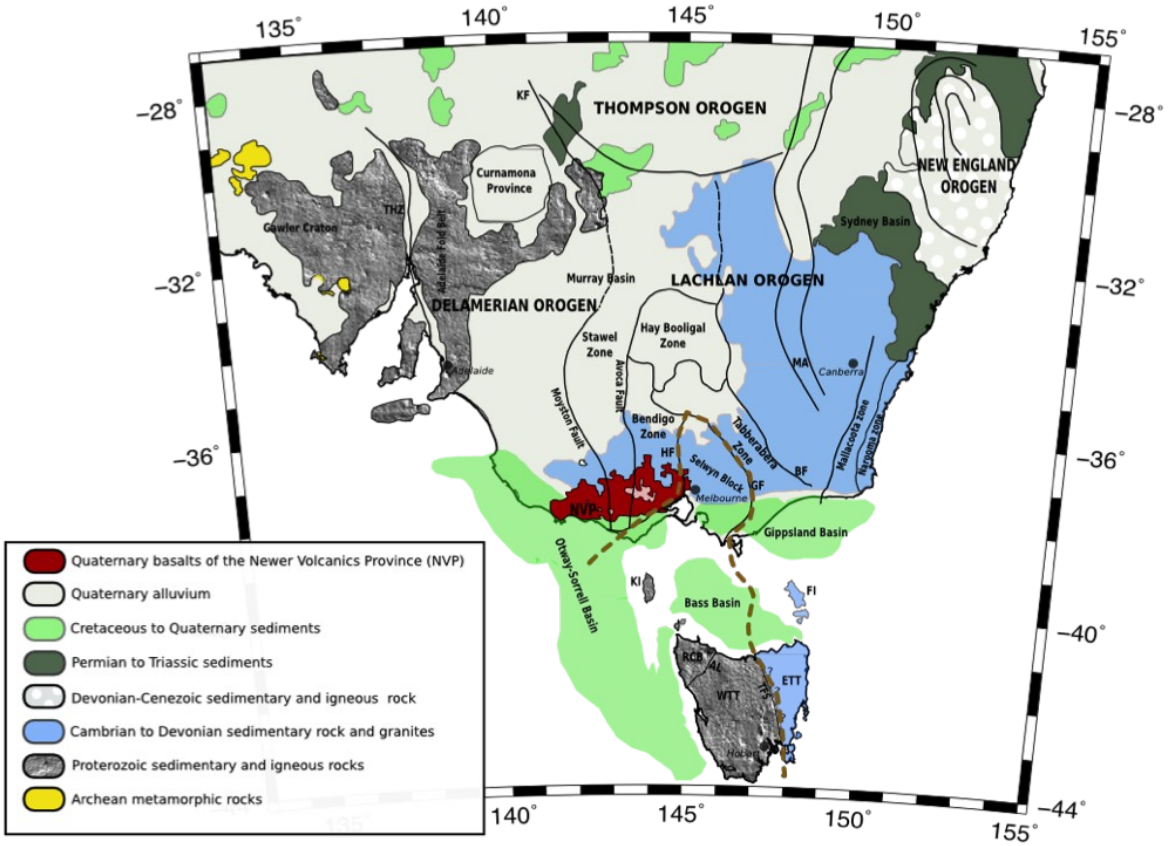

Figure 1: Regional map of southeastern Australia that shows key geological boundaries and the location of observed or inferred tectonic units (mModified from Bello et al., 2019a). Thick black lines delineate structural boundaries and the thick brown dashed line traces out the boundary of VanDieland.– HF = Heathcote Fault; GF = Governor Fault; BF = Bootheragandra Fault; KF = Koonenberry Fault; THZ = Torrens Hinge Zone; MA = Macquarie Arc, NVP = Newer Volcanics Province;; KI = King Island and FI = Flinders Island in Bass Strait; WTT = West Tasmania Terrane; ETT = East Tasmania Terrane; AL = Arthur Lineament; TFS = Tamar Fracture System and RCB = Rocky Cape Block. Outcrop boundaries are sourced from Rawlinson et al. 2016.

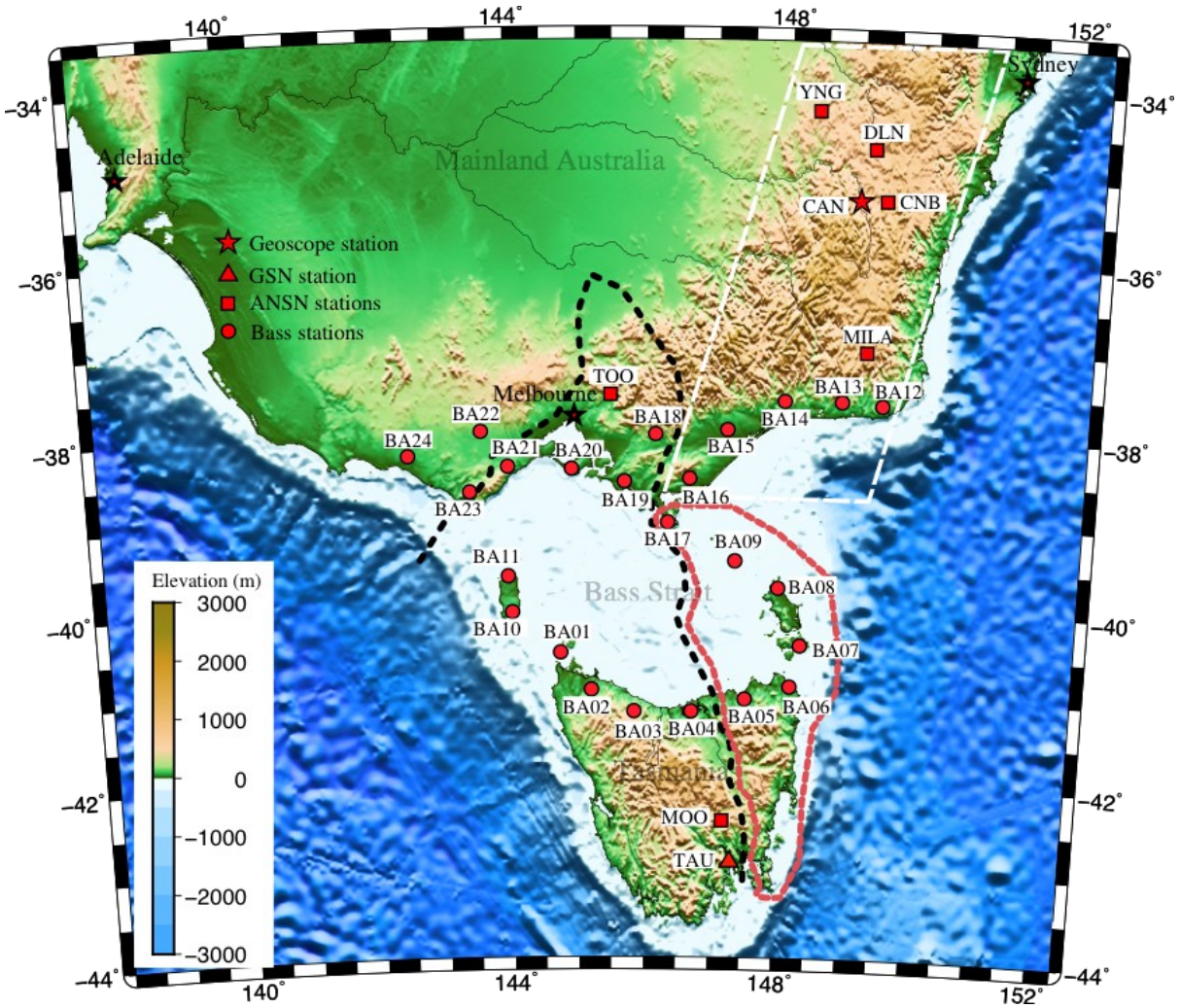

Figure 2: Location of seismic stations used in this study superimposed on a topographic/bathymetric map of southeast Australia (m~~M~~odifued from Bello et al., 2019a). The boundary of VanDieland is delineated by a thick black dashed line. Thick red dashed line outlines the boundary of the East Tasmania Terrane and Furneaux Islands. Thick white dashed line highlights the eastern sector of the Lachlan Fold Belt. Topography/bathymetry is based on the ETOPO~~topo~~1 dataset (Amante and Eakins, 2009).

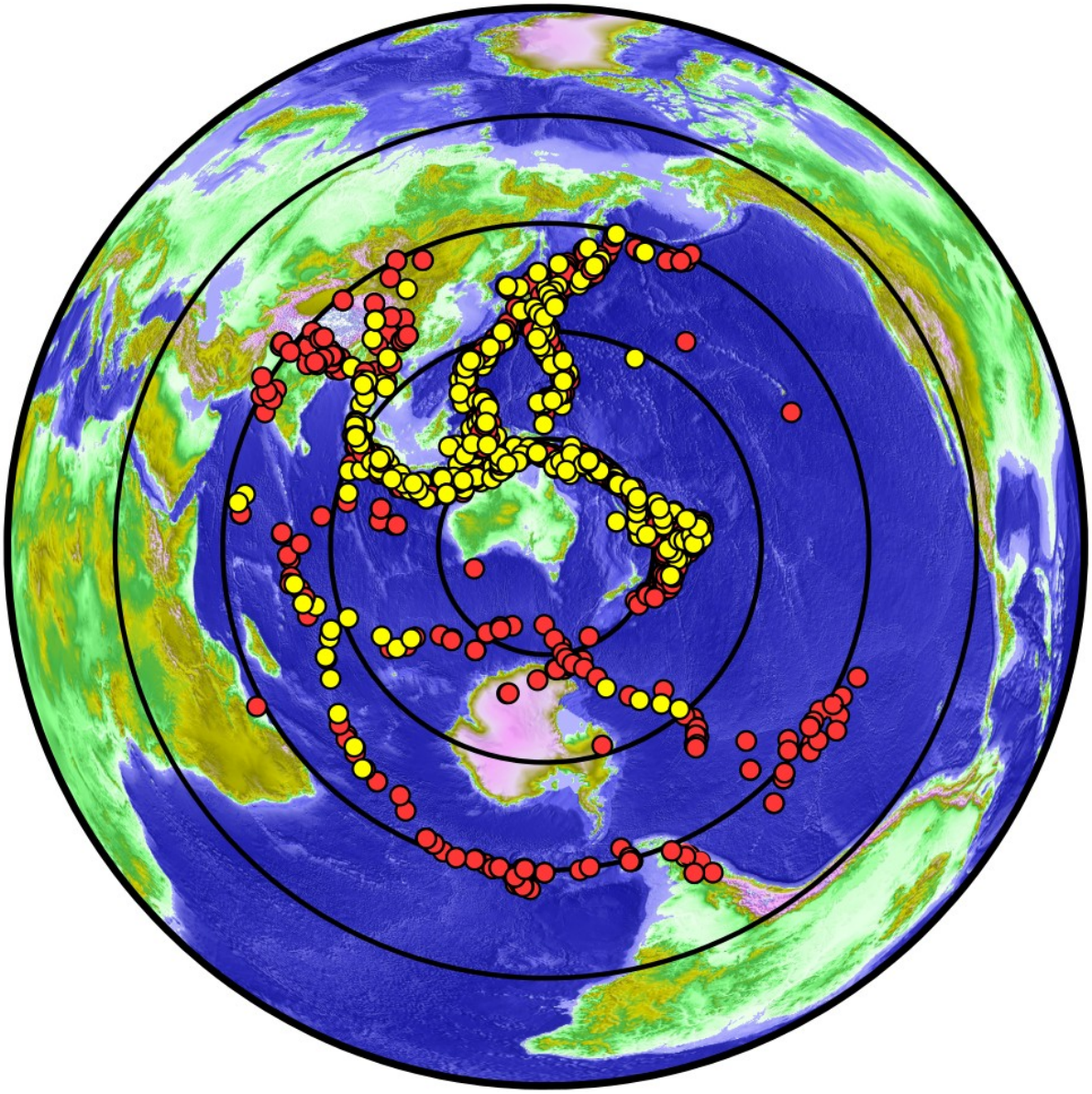

Figure 3: Distribution of distant earthquakes (teleseisms) used in this study. The locations of events that are ultimately used for RF analysis are denoted by yellow dots. Concentric circles are plotted at 30° intervals from the centre of Bass Strait. Topography/bathymetry colours are ~~is~~ based on the Etopo1 dataset (Amante and Eakins, 2009).

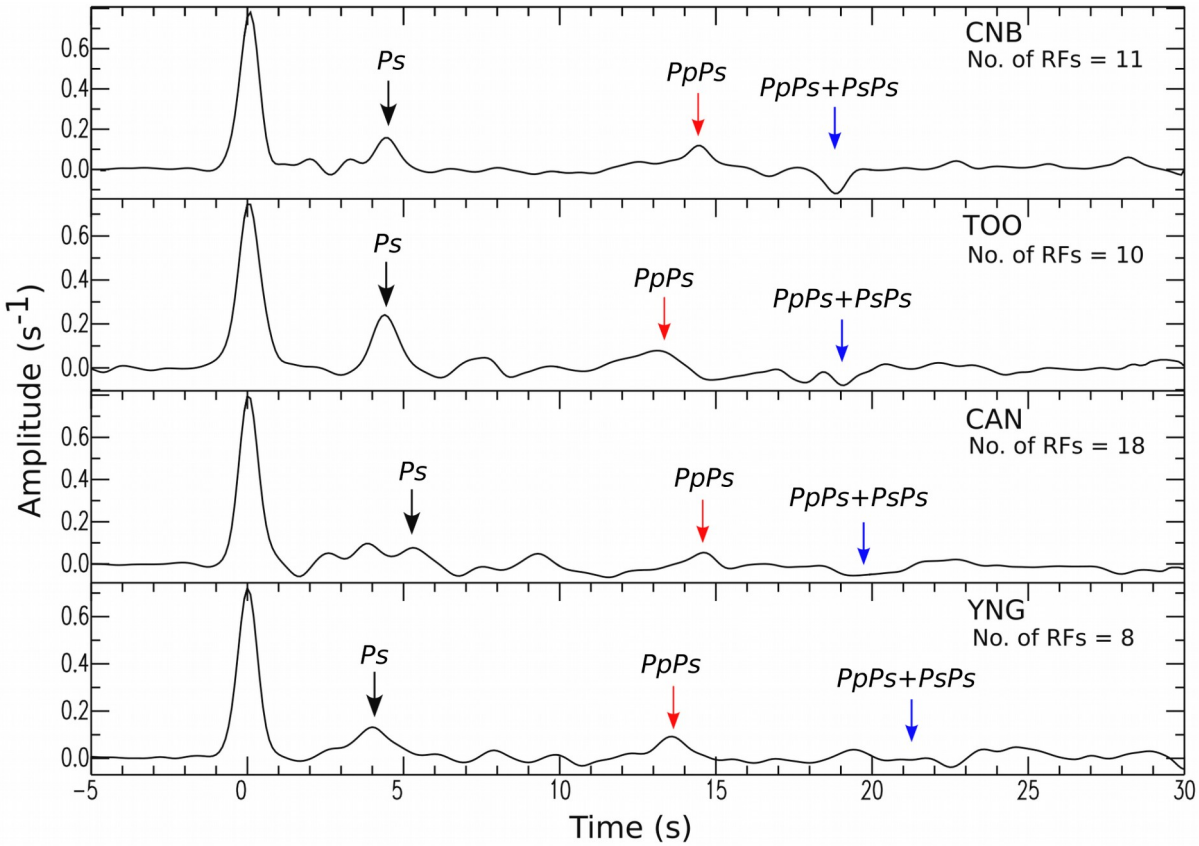

Figure 4: Stacked receiver functions from Australian National Seismic Network (ANSN) stations TOO, YNG, MOO and GSN station TAU. Small arrows indicate arrival of the *Ps* (black), *PpPs* (red) and *PpPs* + *PsPs* (blue) phases from the Moho.

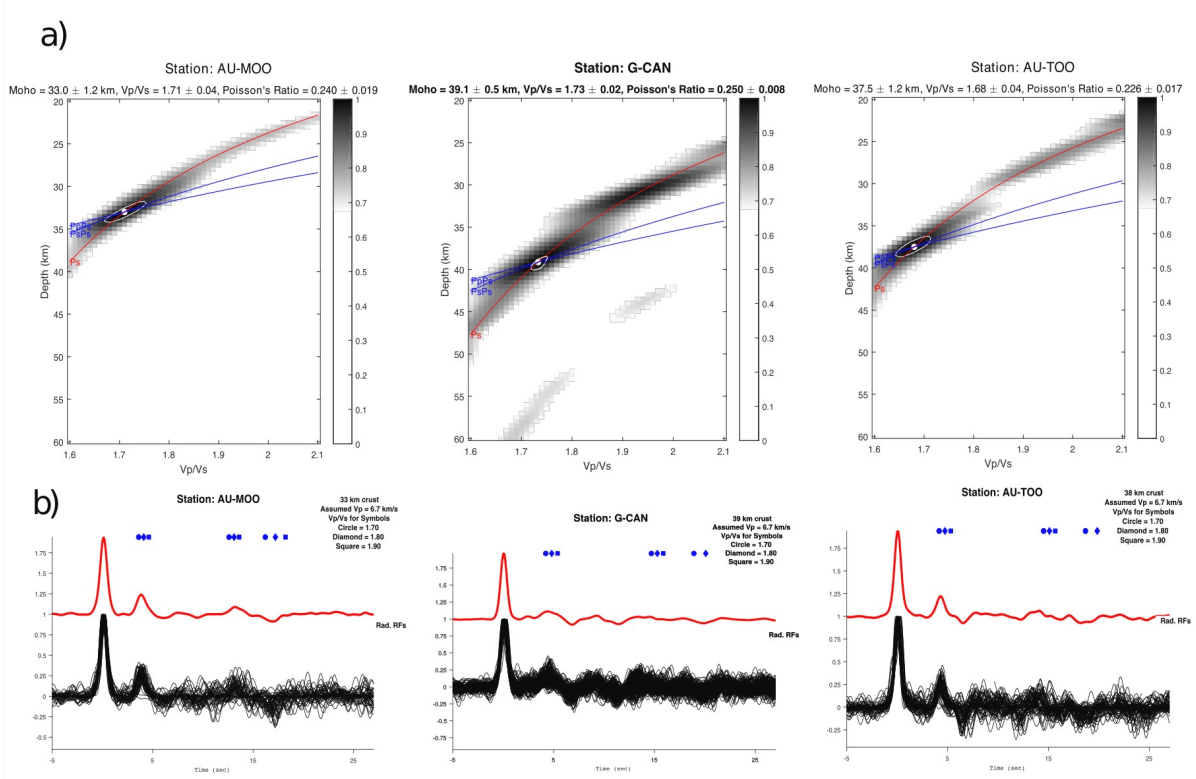

Figure 5: Results from the *H-κ* stacking analysis for RFs (Zhu and Kanamori, 2000) at stations MOO, CAN and TOO. In each case (a) n~~N~~ormalised amplitudes of the stack over all back-azimuths along the travel time curves corresponding to the *Ps* and *PpPs* phases. (b) Corresponding stacked receiver function for each station.

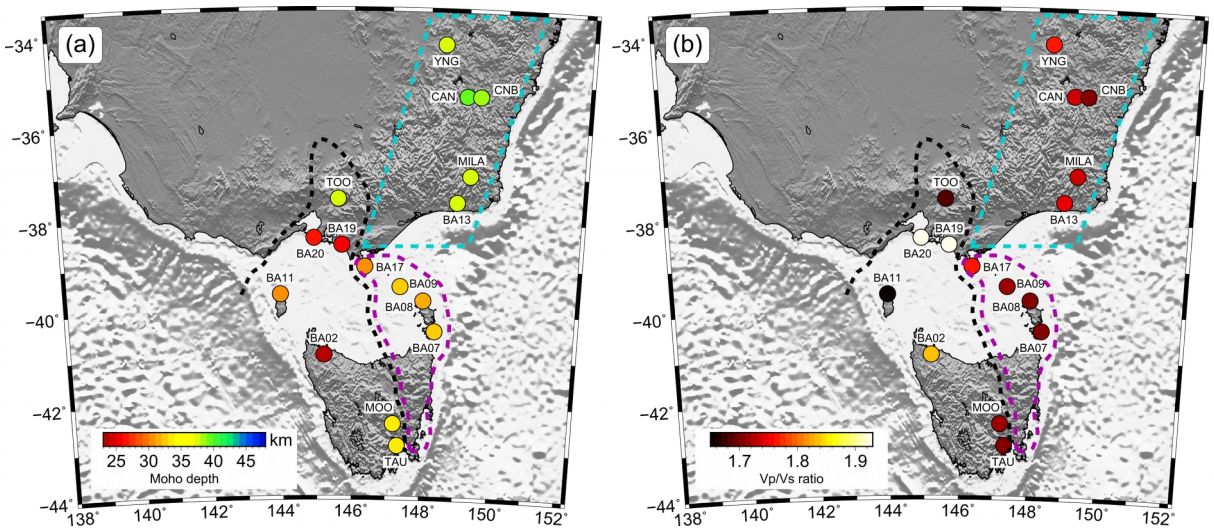

Figure 6: (a) Variations in crustal thickness and (b) *Vp/Vs* ratio taken from the linear (*H-κ*) stacking results (Table 2). Crustal thickness varies between ~2330.5 ± 0.1 km and and 39.1 ± 0.5 km. Thinner crust in Bass Strait can be seen flanked by a relatively thicker crust to the north and south. *Vp/Vs* ratios vary from ~1.655 ± 0.02 to 1.75 ± 0.02 to 1.93. Thick black dashed line denotes the boundary of VanDieland. Thick magentared dashed line outlines the boundary of East Tasmania Terrane and eastern Bass Strait (ETT+EB). Thick cyanwhite dashed line highlights the eastern part of the Lachlan Fold Belt. Illuminated tTopography/bathymetry is based on the Etopo1 dataset (Amante and Eakins, 2009).

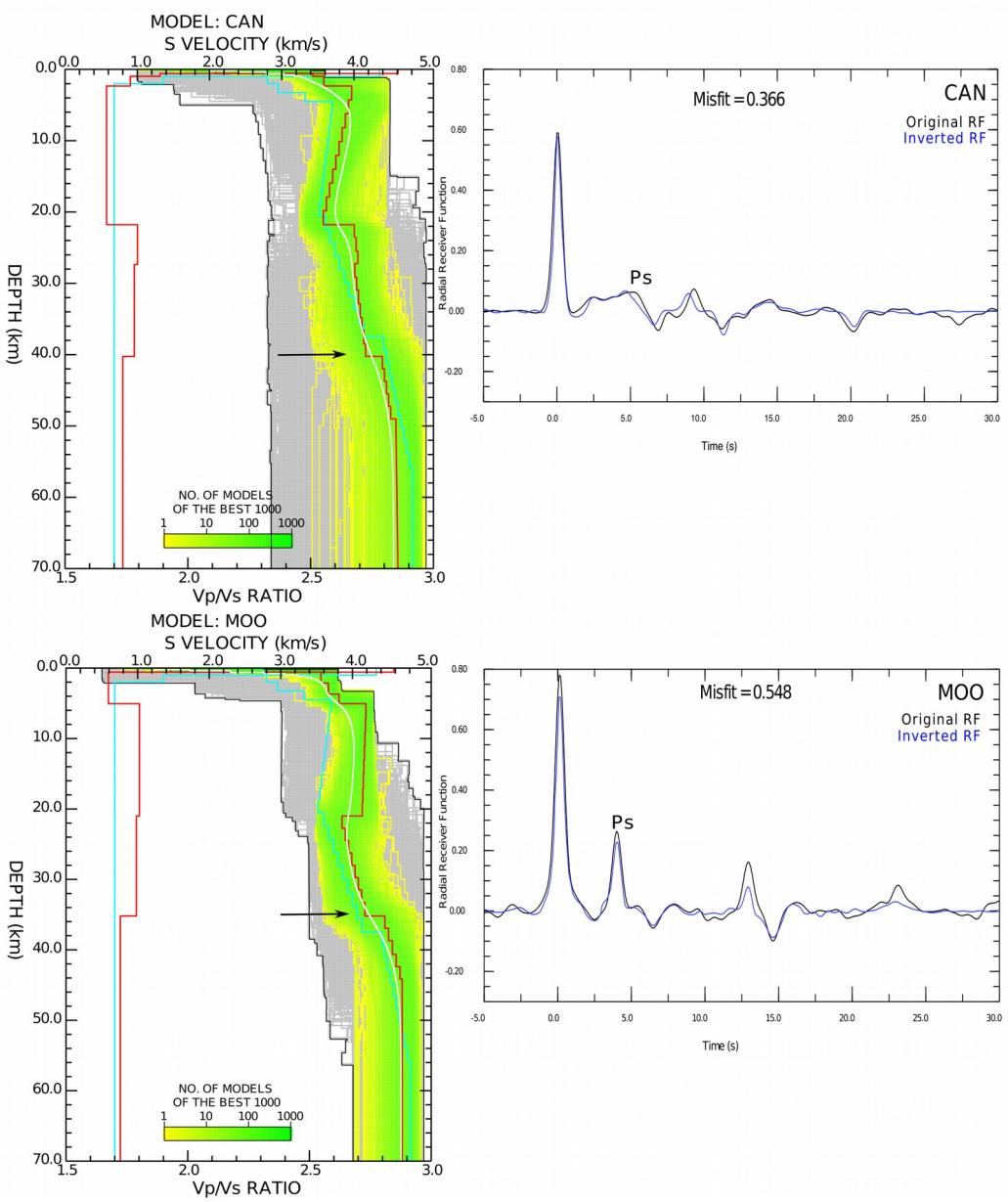

Figure 7: (Left) Seismic velocity models for CAN and MOO stations obtained from the neighbourhood algorithm (Sambridge 1999a). The grey area indicates all the models searched by the algorithm. The best 1000 models are indicated by the yellow to green colours; the best one (smallest misfit) corresponds to the red line, both for *S*-wave velocity (top horizontal axis) and *Vp/Vs* ratio (bottom horizontal axis) and the white line is the average velocity model. (Right) Waveform matches between the observed stacked receiver functions (black) and predictions (blue) based on the best models. "Misfit" refers to the chi-square estimate as defined by Equation 2.

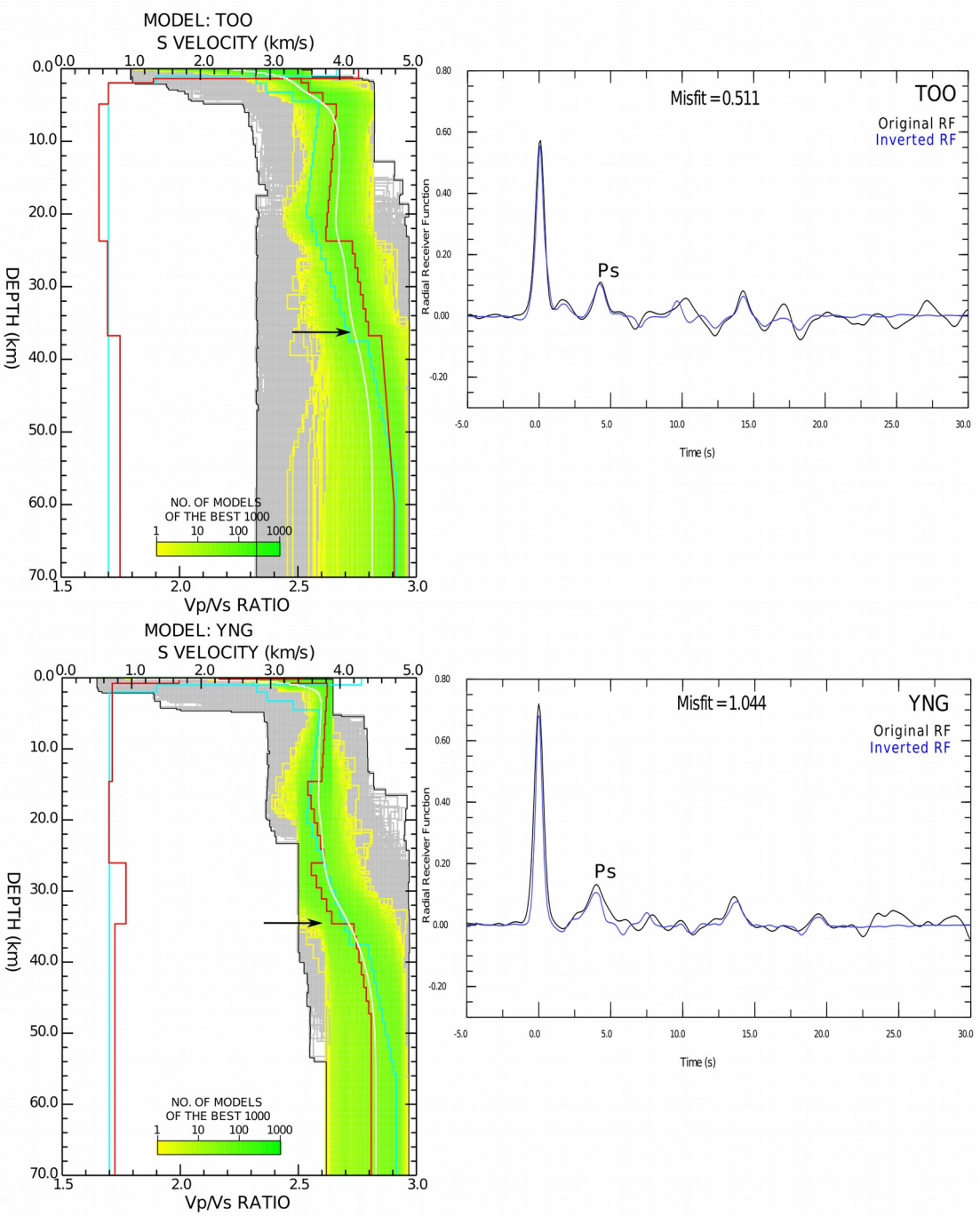

Figure 8: (Left) Seismic velocity models for stations TOO and YNG obtained from the neighbourhood algorithm. (Right) Comparison between the observed stacked and the predicted receiver functions from the NA inversion. See Figure 7 caption for more details.

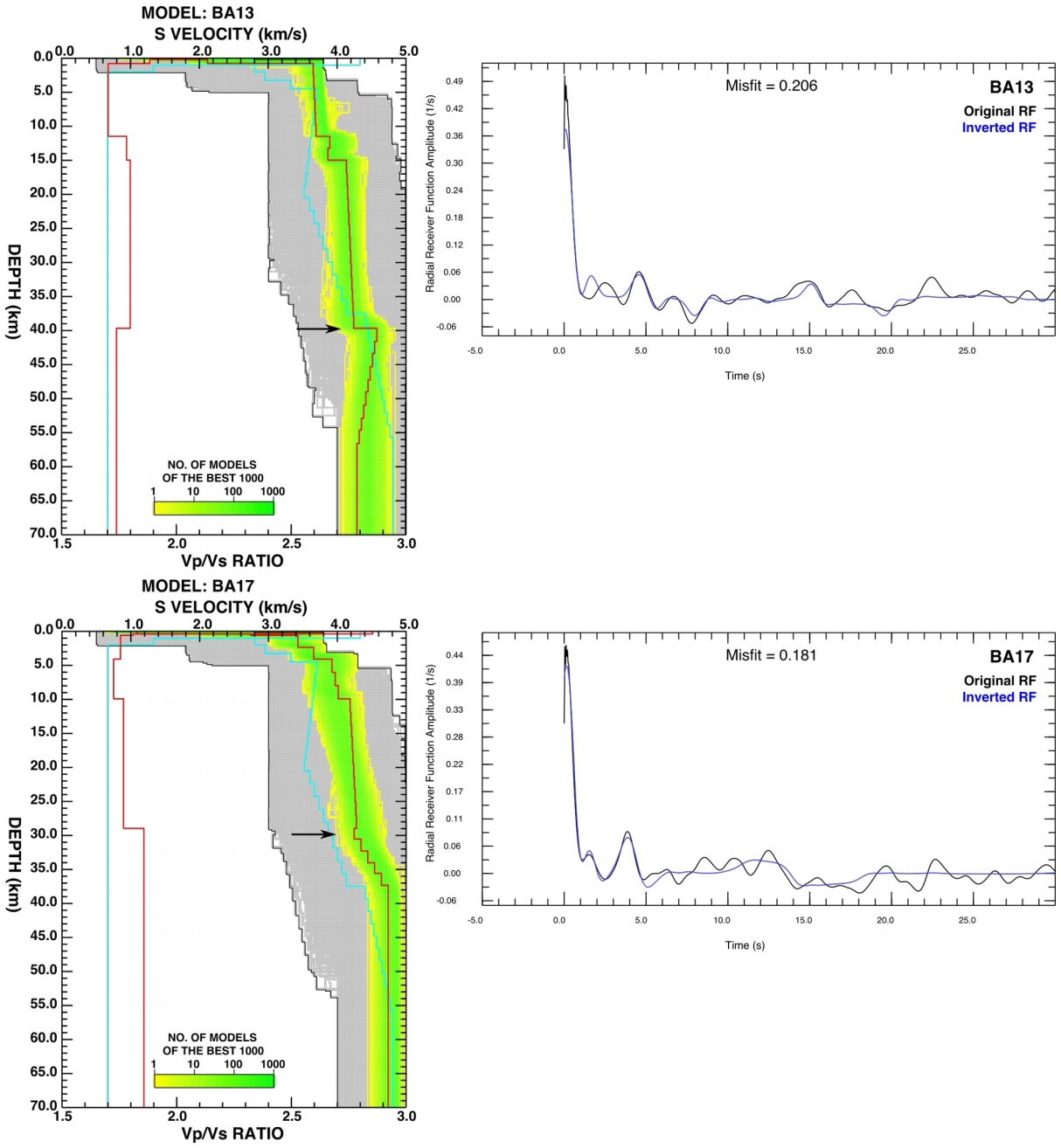

Figure 9: (Left) Seismic velocity models for temporary stations BA13 and BA17 obtained from the neighbourhood algorithm. (Right) Comparison between the observed stacked and the predicted receiver functions from the NA inversion. See Figure 7 caption for more details.

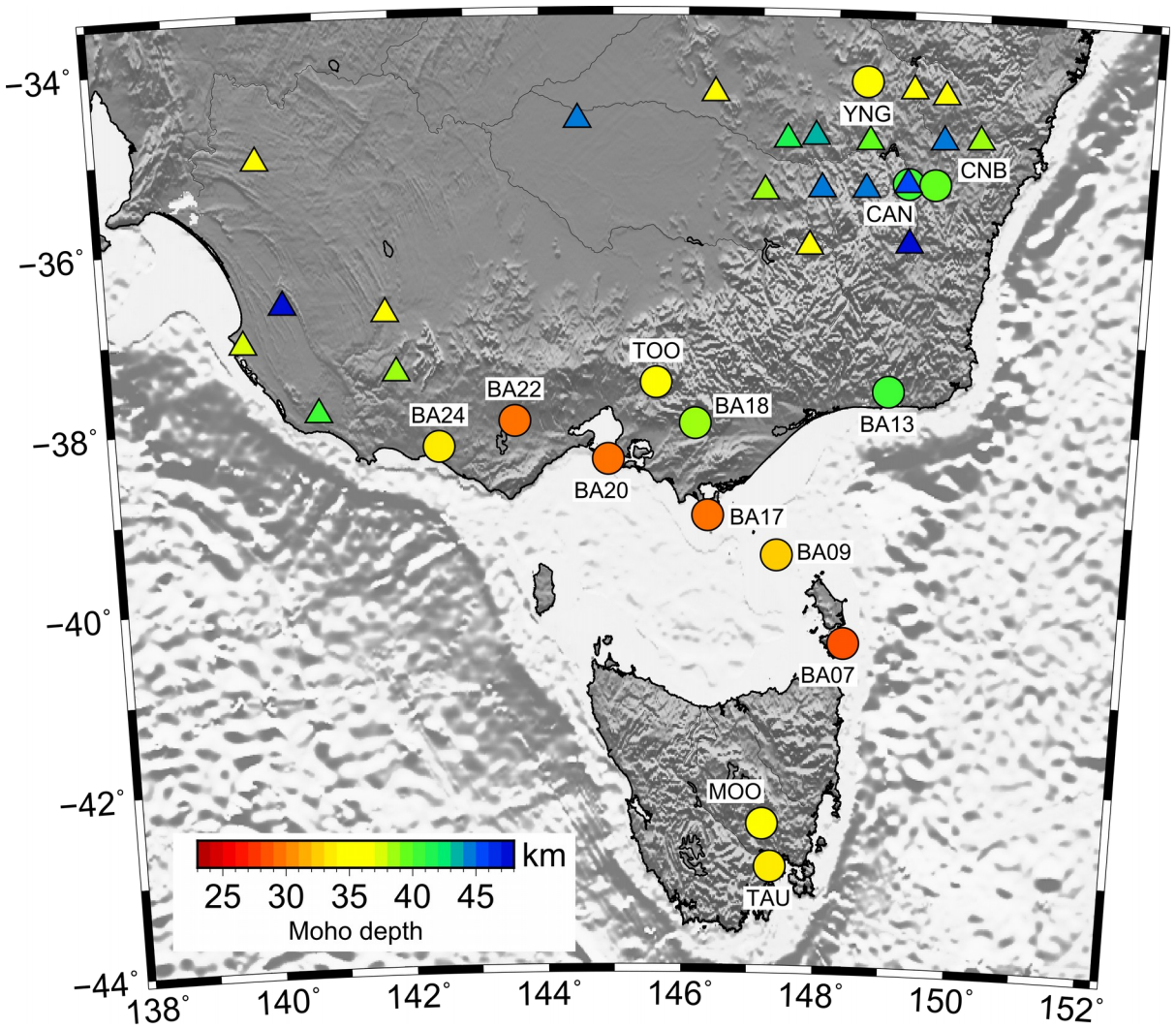

Figure 10: ~~(a)~~ Map showing crustal thickness variations based on the S-wave velocity inversion results of this study (stars) and previous studies (octagons) (Clitheroe et al., 2000, Fontaine et al., 2013a,b; Shibitani, 1996; ~~Collins, 1991~~Tkalcic et al, 2013). ~~and (b) comparison of crustal thickness variations based on the *H-κ* grid search results of this study (stars) and previous results from the study of Tkalčić et al. (2012) (octagons).~~ Topography/bathymetry is based on the Etopo1 dataset (Amante and Eakins, 2009).

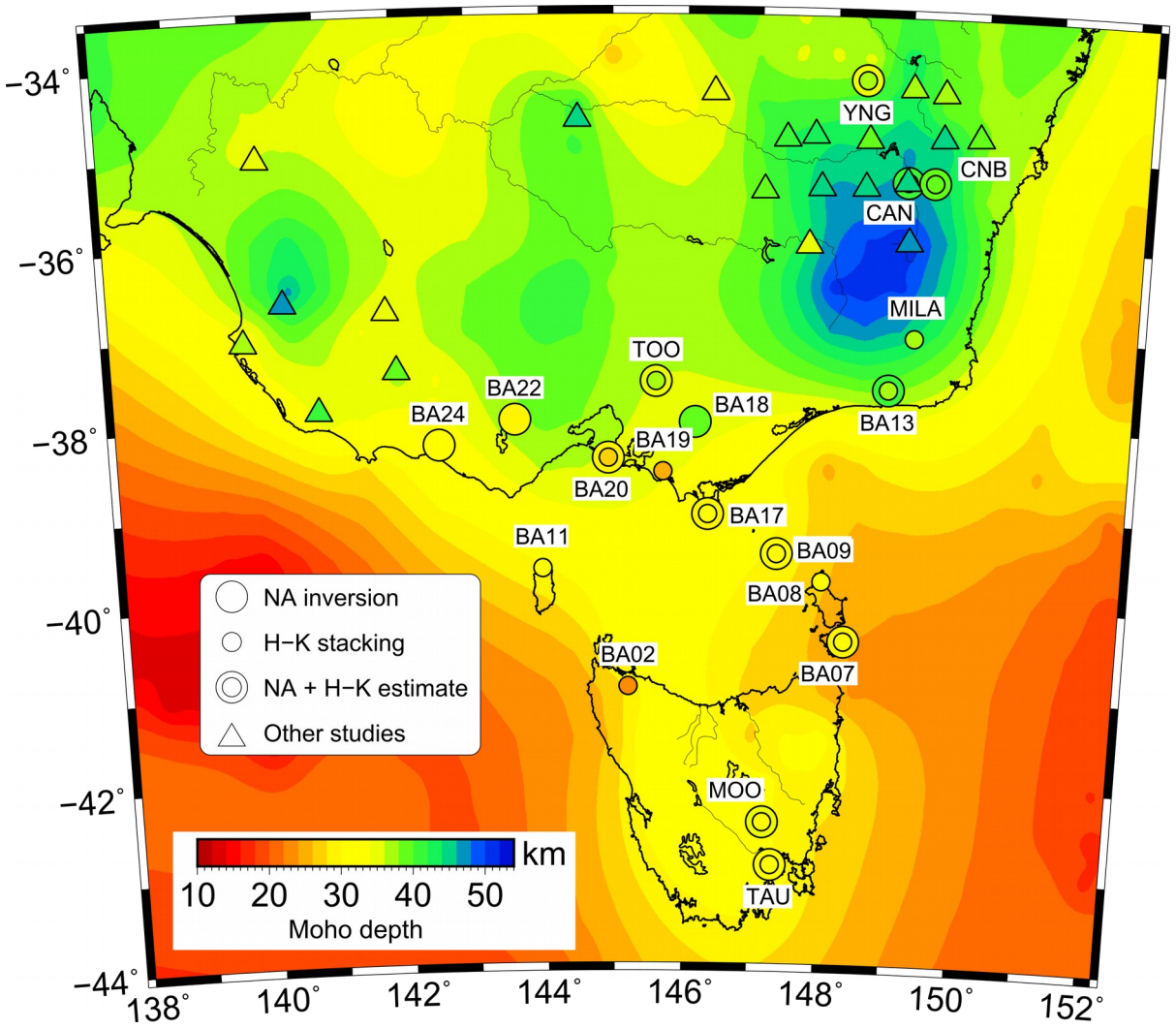

Figure 11: Comparison between the AusMoho model (background colour map) and Moho depths determined through RF analaysis in this and previous studies. Small coloured circles denote the Moho depths determined from H-κ stacking, whereas large coloured circles correspond to receiver function estimates. When both H-κ and NA-derived depths are available at a single station, the smaller H-κ circle is superimposed on the larger NA circle, so that both depths can be observed on the one plot. Moho depths determined from previous RF studies are denoted by triangles.

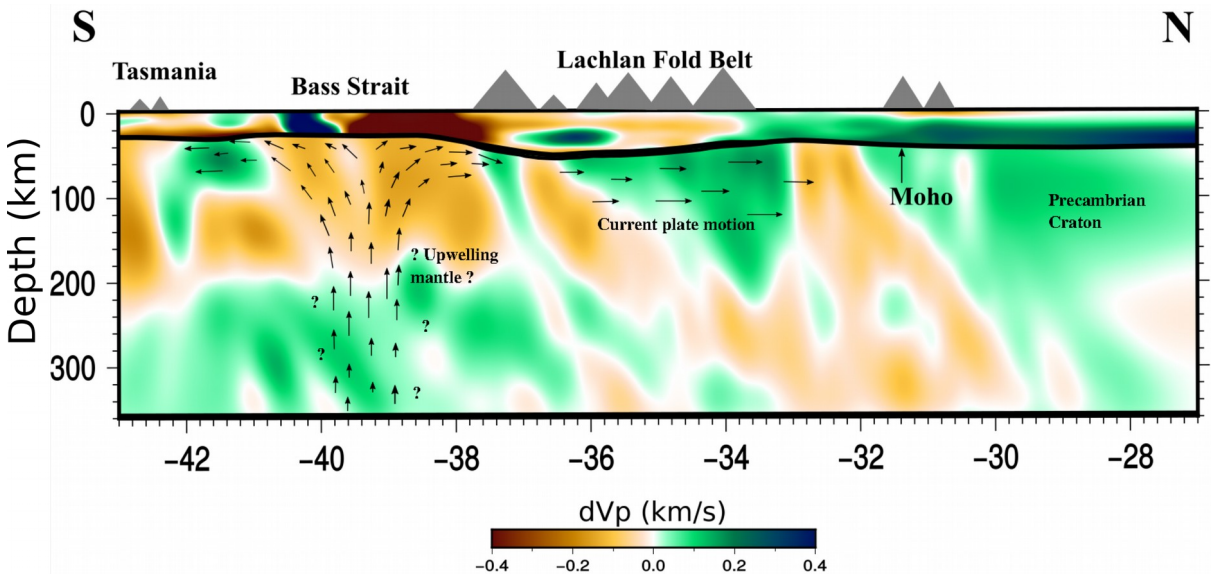

Figure 12: Composite result of teleseismic tomography (mantle velocity anomalies), ambient noise (crustal velocity anomalies), receiver functions (Moho) and shear wave splitting (inferred mantle flow relative to over-riding plate). Velocity slices are taken at 148°E.

Supplementary Information to
“Crustal structure of southeast Australia from teleseismic receiver functions”

Mohammed Bello[1, 2], David G. Cornwell[1], Nicholas Rawlinson[3], Anya M. Reading[4], Othaniel K. Likkason[2]

[1]Department Geology & Geophysics, University of Aberdeen, Aberdeen, UK
[2]Department of Physics, Abubakar Tafawa Balewa University, Bauchi, Nigeria
[3]Department of Earth Sciences, University of Cambridge, UK
[4]School of Natural Sciences (Physics), University of Tasmania, Australia

Correspondence to: Mohammed Bello (mbazare13@yahoo.com)

Contents

Introduction

This supplementary material presents H- κ stacks and 1-D NA inversion results that are not presented in the main text. It also includes a comparison of Moho depths beneath Tasmania.

H-κ stacking analysis

In this section, results from the H-κ stacking analysis for RFs at stations listed in Table 2 of the main text are presented. In each case, one panel represents the normalised amplitudes of the stack over all back-azimuths along the travel time curves corresponding to the Ps and PpP s + PsPs phases. The other panel is the corresponding stacked receiver function for the station.

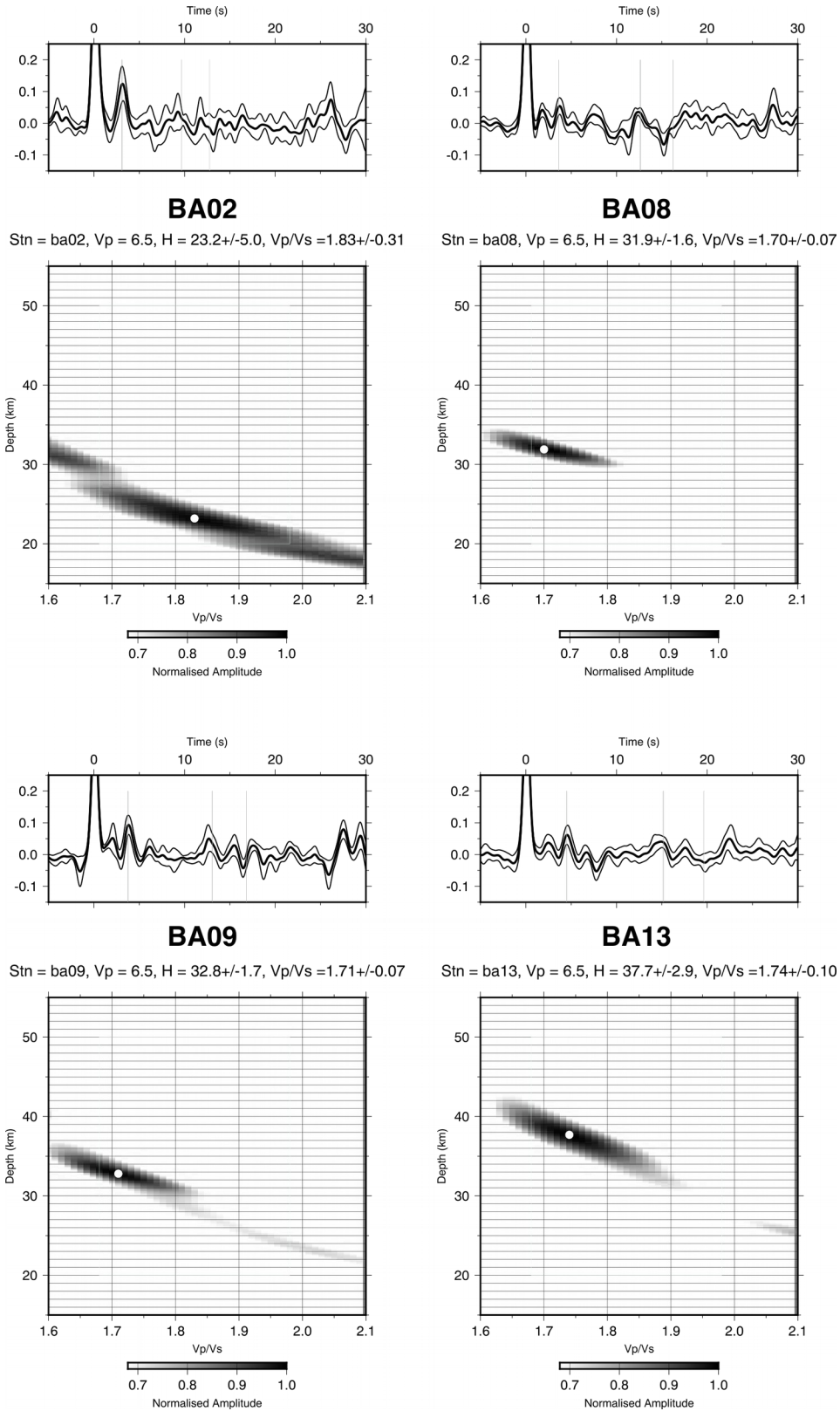

Figure S1: H-κ stacking results for stations BA02, BA08, BA09 and BA13 from the temporary network.

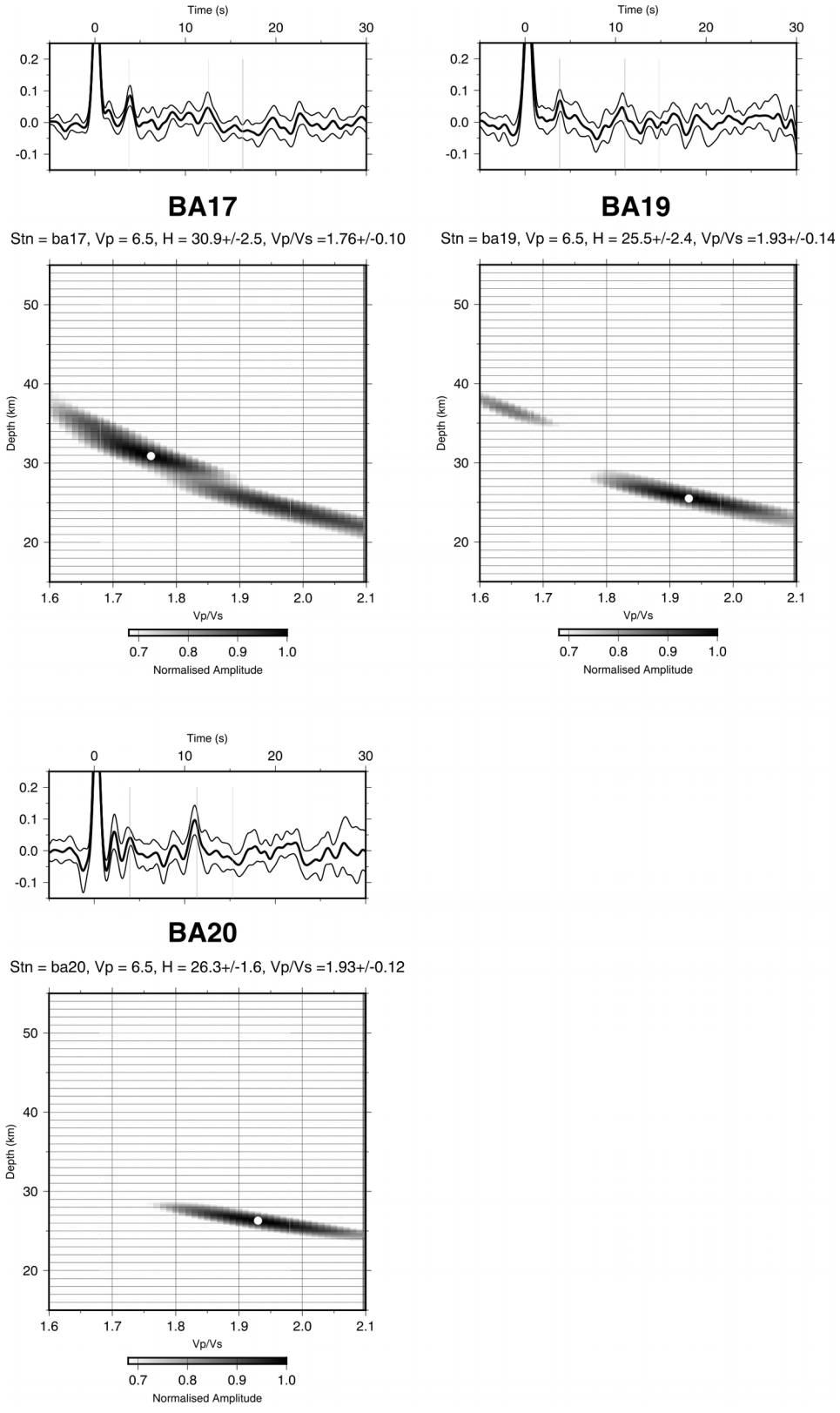

Figure S2: H-κ stacking results for stations BA17, BA19 and BA20 from the temporary network.

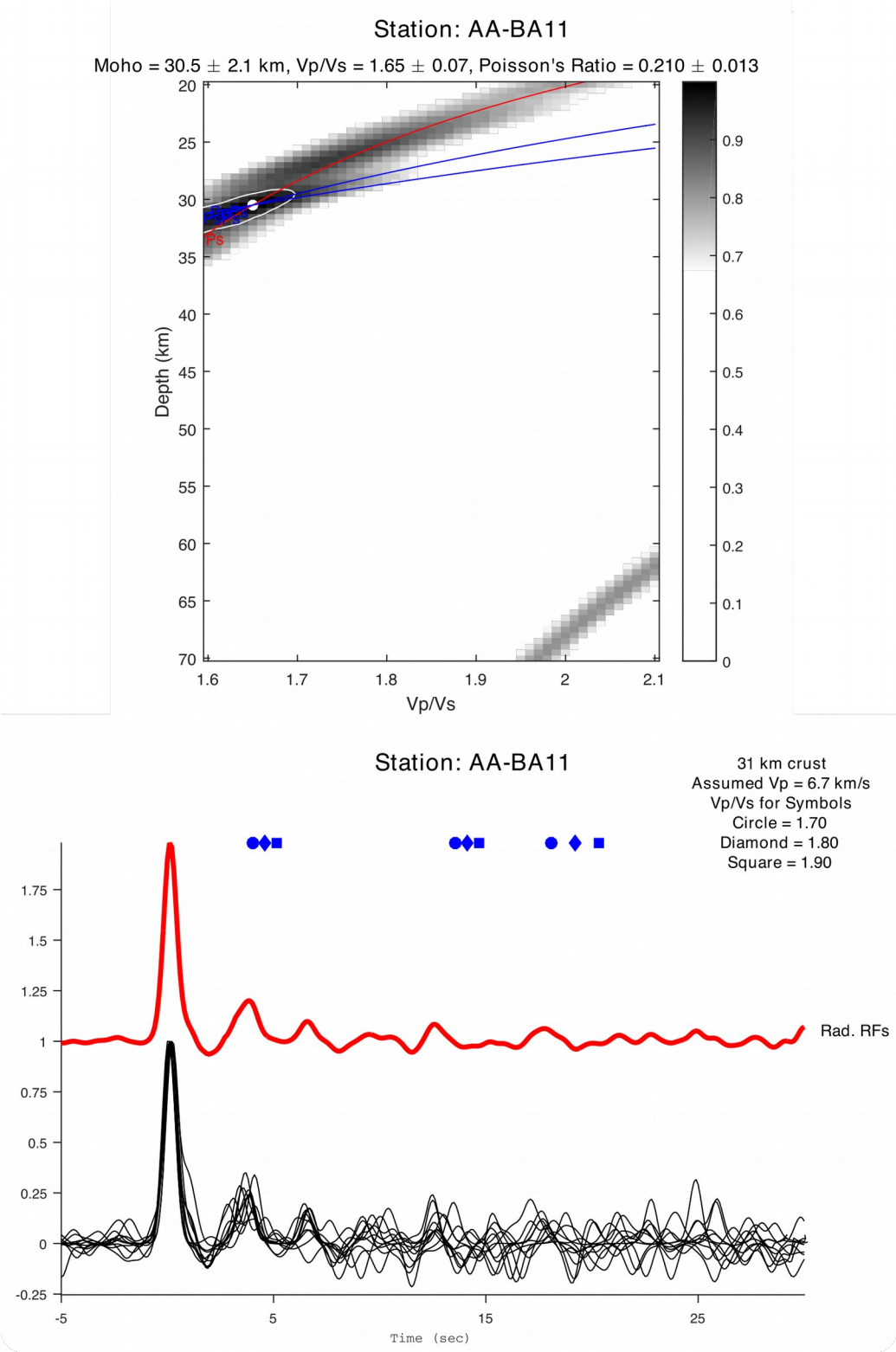

Figure S3: H-κ stacking results for station BA11 from the temporary network.

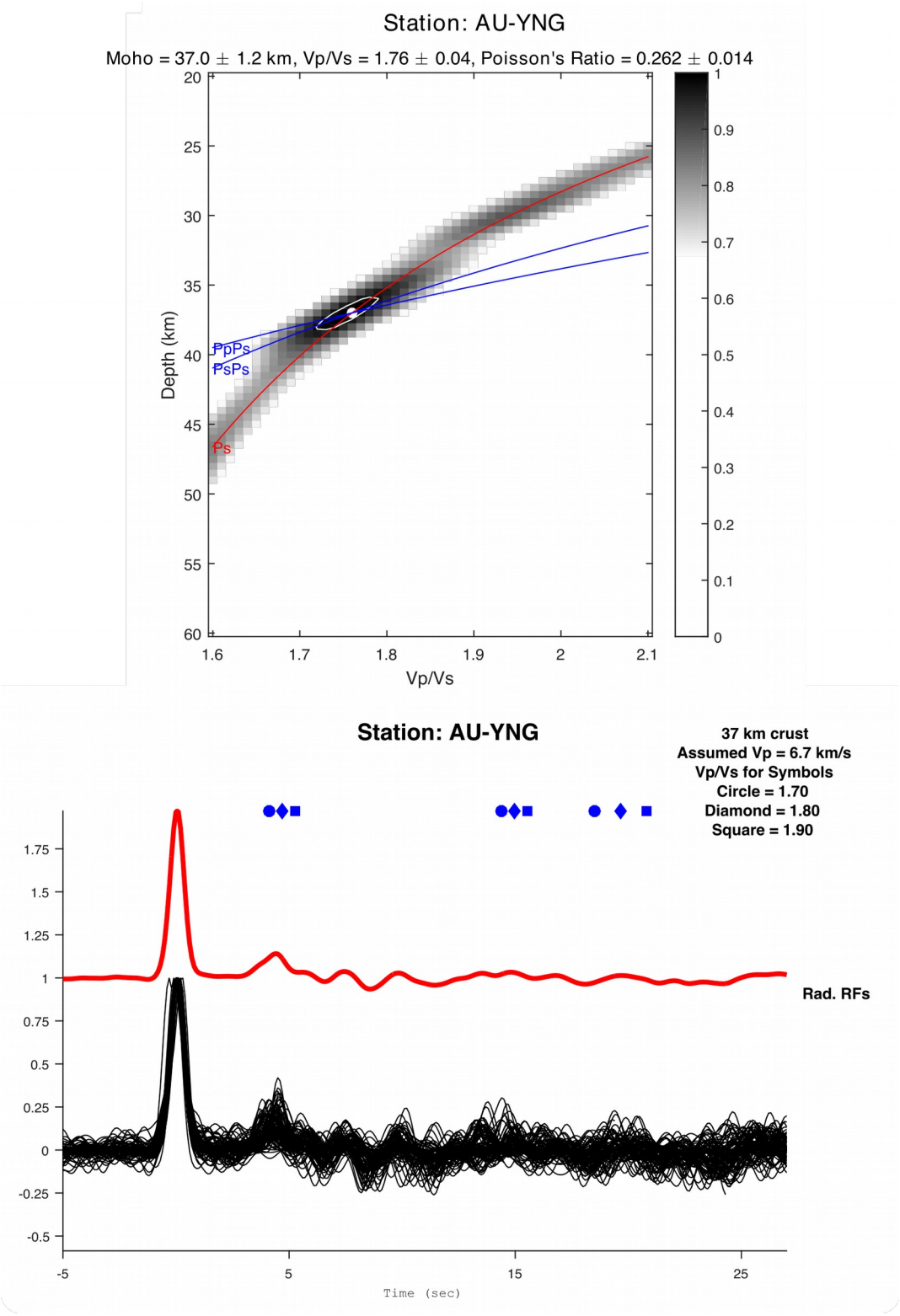

Figure S4: H-κ stacking results for permanent station YNG.

1-D S-wave velocity inversion

This section presents seismic S-wave velocity models for stations listed in Table 2, except those already shown in the main manuscript, obtained from receiver function inversion using the neighbourhood algorithm. The grey area indicates all the models searched by the algorithm. The best 1000 models are indicated in the yellow to green colour; the best model (smallest misfit) corresponds to the red line, both for S-wave velocity and *Vp/Vs* ratio, whereas the white line is the average velocity model computed from the best 1000 models. (Right) Waveform matches between the observed stacked receiver functions (black) and prediction (grey) based on the average of the best 1000 models.

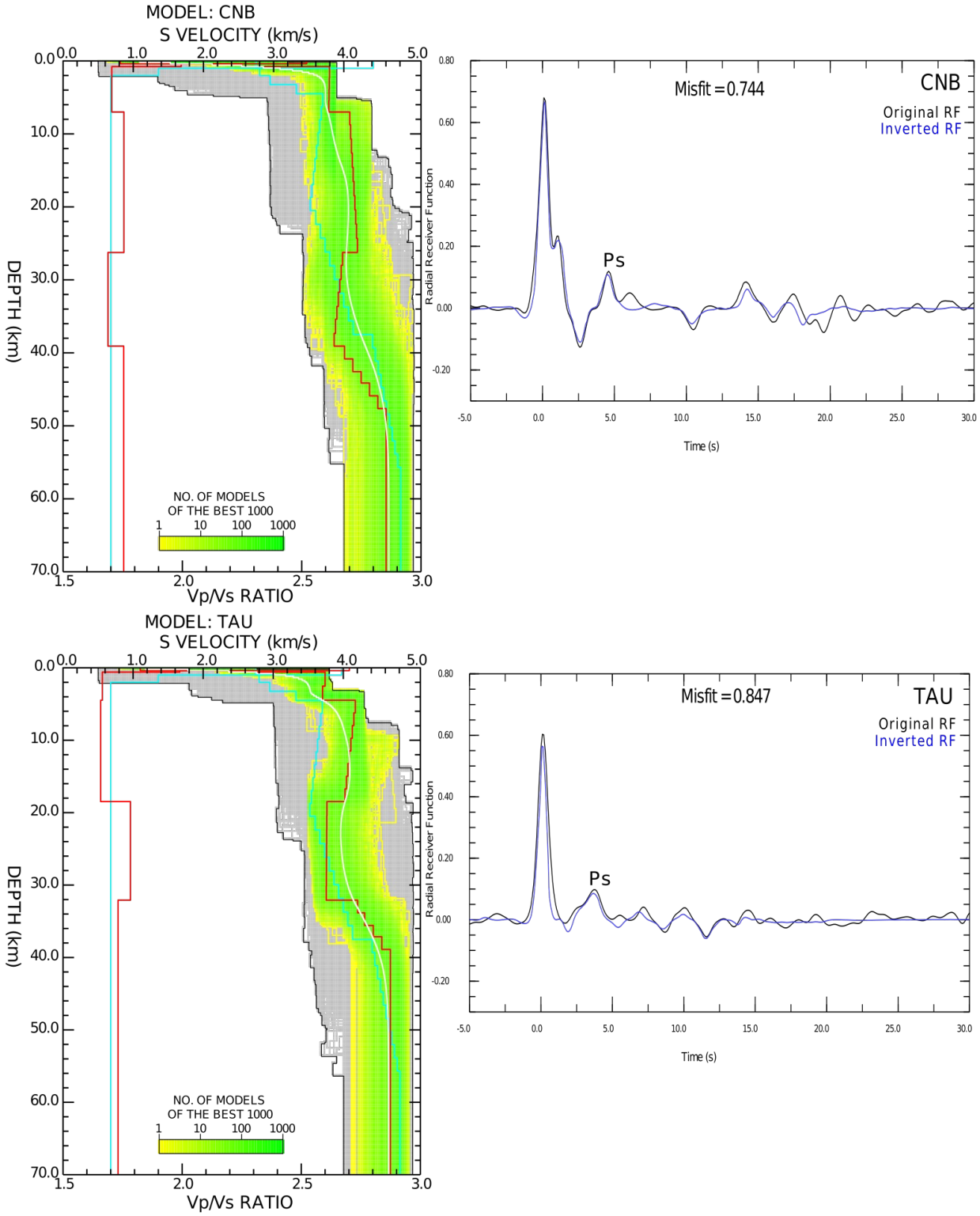

Figure S5: (Left) Density plot of S-wave velocity models and (right) observed and synthetic RF plots for stations CNB and TAU

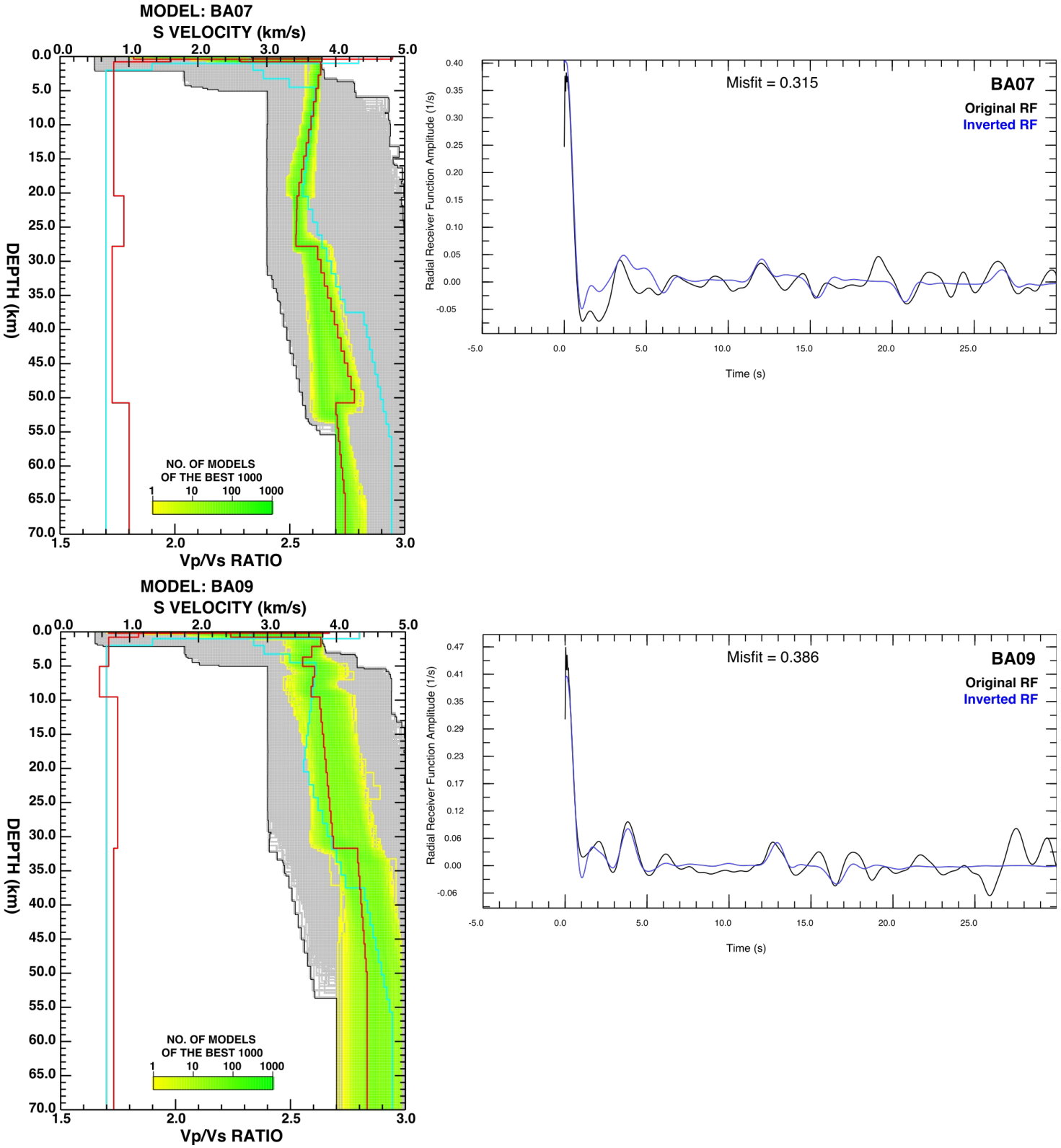

Figure S6: (Left) Density plot of S-wave velocity models and (right) observed and synthetic RF plots for stations BA07 and BA09.

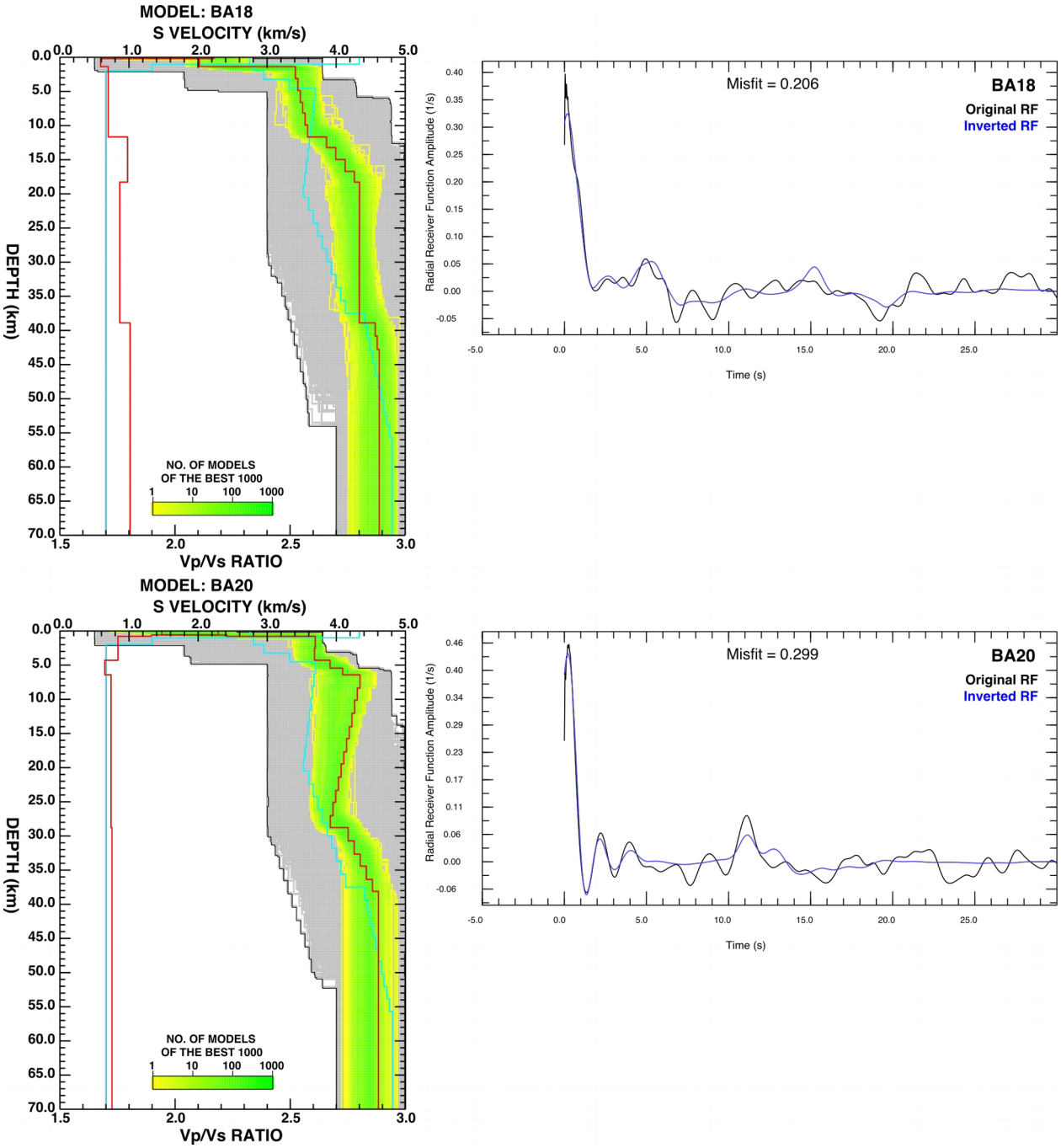

Figure S7: (Left) Density plot of S-wave velocity models and (right) observed and synthetic RF plots for stations BA18 and BA20.

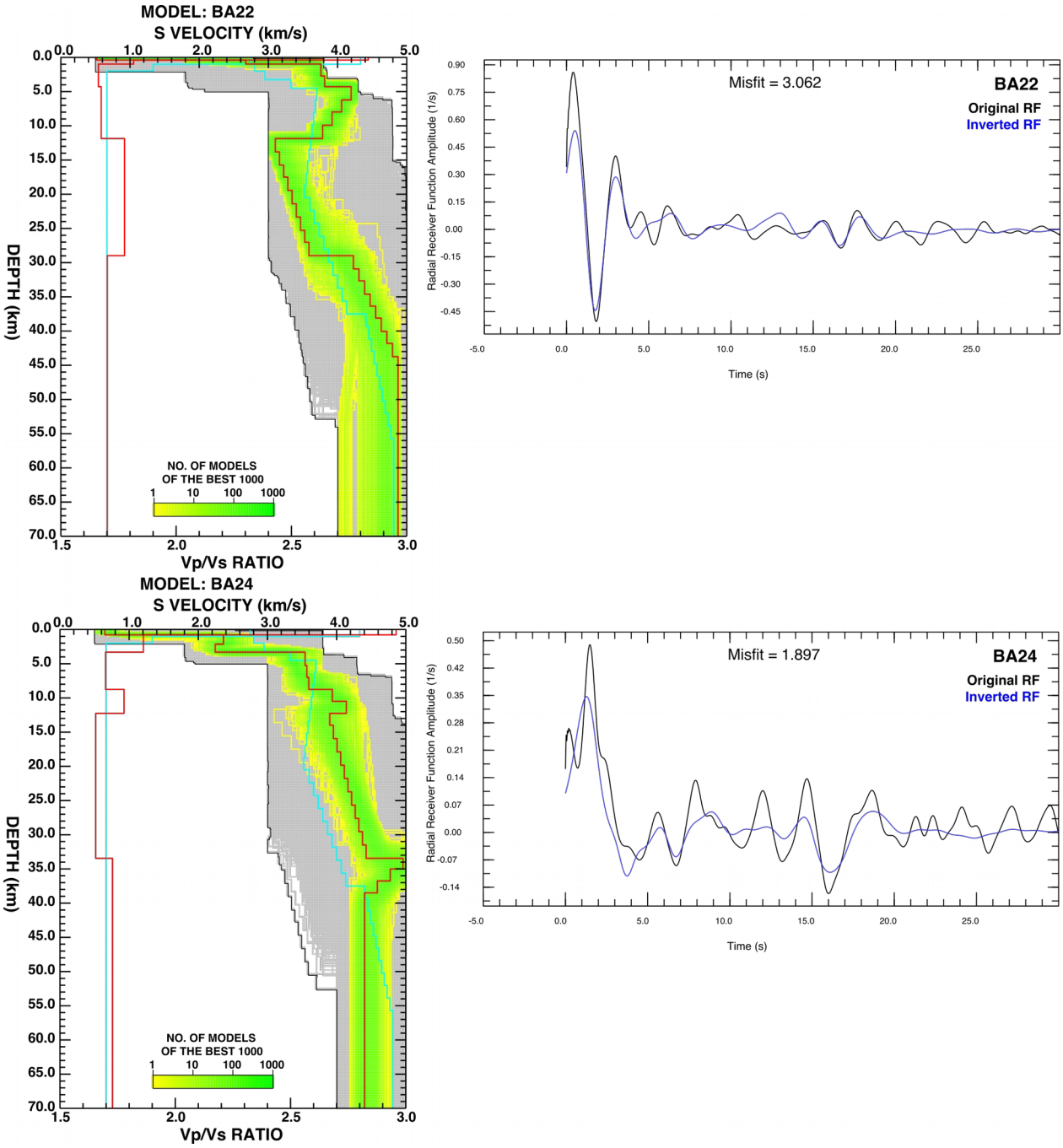

Figure S8: (Left) Density plot of S-wave velocity models and (right) observed and synthetic RF plots for stations BA07 and BA09.

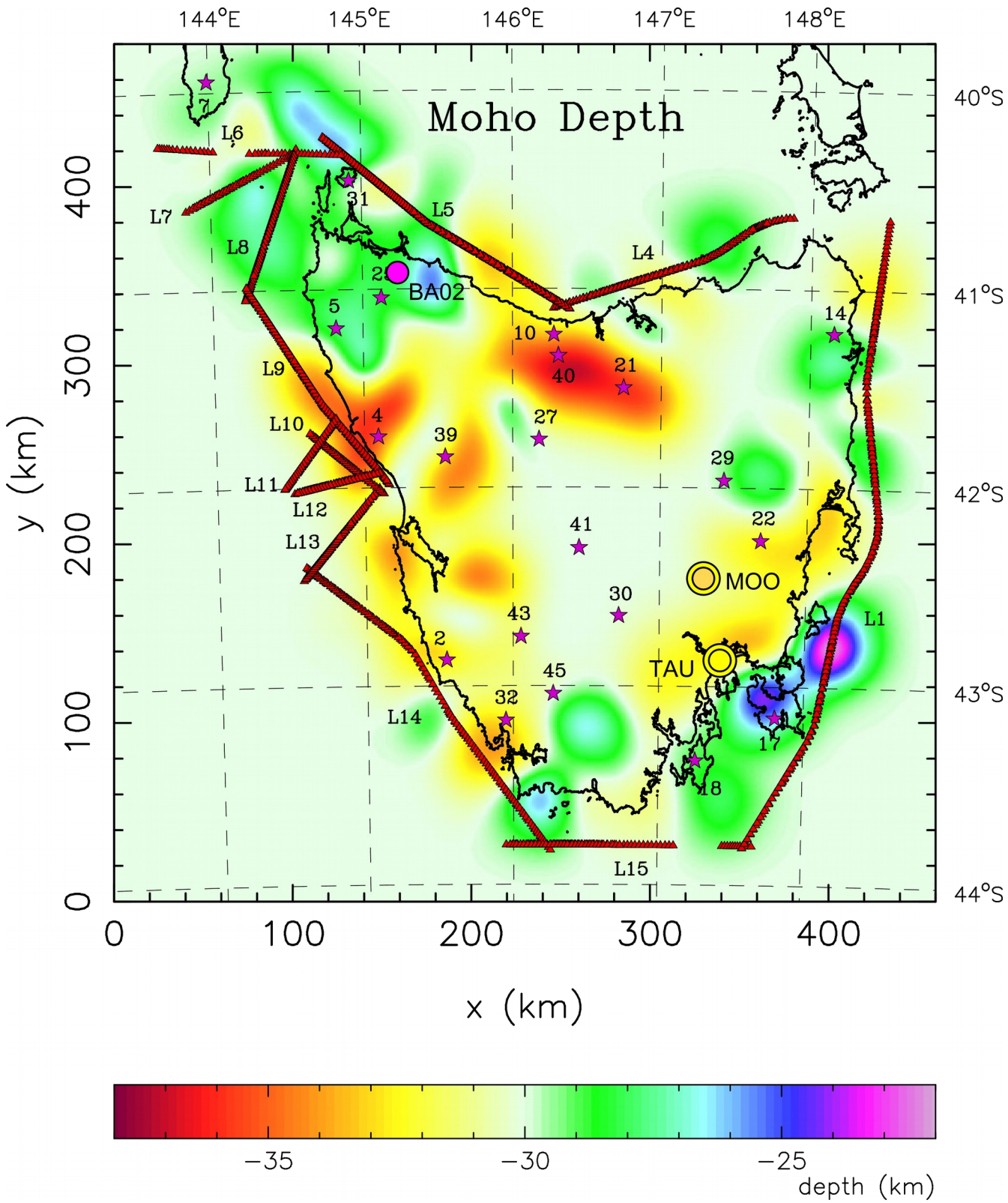

Figure S9: Comparison between Moho map of Rawlinson et al. (2001) and receiver function results from this study. Small circles correspond to results from H-κ stacking, and large circles correspond to results from NA inversion.